

Impacts of regional uplift of the Tibetan Plateau on local summer precipitation and downstream moisture budget: A simulation study

Kai Yang^{1,2} | Jinghua Chen^{1,2} | Chunsong Lu^{1,2} | Junjun Li^{1,2} |
 Tianyu Liu^{1,2} | Liping Deng³ | Yanwei Li^{1,2}

¹Collaborative Innovation Center on Forecast and Evaluation of Meteorological Disasters (CIC-FEMD), Nanjing University of Information Science & Technology, Nanjing, China

²Key Laboratory for Aerosol-Cloud-Precipitation of China Meteorological Administration, School of Atmospheric Physics, Nanjing University of Information Science & Technology, Nanjing, China

³College of Ocean and Meteorology, Guangdong Ocean University, Zhanjiang, China

Correspondence

Jinghua Chen, Key Laboratory for Aerosol-Cloud-Precipitation of China Meteorological Administration, School of Atmospheric Physics, Nanjing University of Information Science & Technology, Nanjing 210044, China.
 Email: jhchen@nuist.edu.cn

Funding information

Natural Science Foundation of Jiangsu Province, Grant/Award Number: BK20170945; Second Tibetan Plateau Scientific Expedition and Research (STEP) program, Grant/Award Number: 2019QZKK0105; National Science Foundation of China, Grant/Award Numbers: 41875071, 42075068, 42075067

Abstract

Using the Weather Research and Forecasting (WRF) model, a series of sensitivity experiments were conducted to study the individual and overall effects of the various topographic uplifts of the Tibetan Plateau (TP) on regional climate variability. The presence of the southern slope of the TP facilitates the maintenance and development of the South Asia High (SAH), which produces a positive cyclic response between local precipitation and SAH, so that the northern branch of the South Asian summer monsoon (SASM) maintains the water vapor supply. At the same time, the southern slope of the TP has a positive effect on the mid-latitude tropospheric anomalous cyclone and anticyclone systems which promotes the downstream advancement of the East Asian summer monsoon (EASM) and is favourable for the transfer of water vapor and convective clouds downstream. The role of the TP platform is mainly due to the lifting of moisture generated by its local heating, which favours the formation of local convective clouds and precipitation while causing nonadiabatic warming of the troposphere. Water vapor transported from the TP could affect precipitation in central-eastern China (CEC). However, the supply of water vapor in Southern East China (SEC) mainly comes from the southeast coast of China. The Tibetan Plateau sensitive areas (TPSA) have impacts on the water vapor transport path. Removing the TPSA favours an increase in precipitation and convective clouds in SEC. The removal of topographic disturbances favours the convergence and dispersion of water vapor at mid-latitudes. The mid-latitude dynamical anomaly may form a standoff with the low-latitude dynamical system. This leads to inefficient precipitation and convective generation processes, a weakened monsoon advance over land, and a southward shift in the rainfall belt.

KEY WORDS

moisture transport, terrain uplift, Tibetan Plateau, Yangtze River Delta

1 | INTRODUCTION

The Tibetan Plateau (TP), the world's third pole, is the highest and most complex plateau globally. The role of

TP topography in the Asian monsoon, regional water and energy cycles has been studied by many scholars (Yeh *et al.*, 1979; Lu *et al.*, 2005; Xu *et al.*, 2008). The particular topography of the TP creates unique thermal and

mechanical effects on atmospheric circulation (Ding and Johnny, 2005; Liu *et al.*, 2007; Molnar *et al.*, 2010; Wu *et al.*, 2014). The thermal effect refers to the heating effect of the TP as an atmospheric heat source in summer (Duan and Wu, 2005; Molnar *et al.*, 2010; Duan *et al.*, 2017). The mechanical effect refers to the blocking effect on the low-level westerly wind in the troposphere caused by the large and high topography of the TP (Wu *et al.*, 2007; Molnar *et al.*, 2010; Chen and Bordoni, 2014). Both data analysis and numerical simulation results indicate that the mechanical and thermal effects of the TP give rise to unique characteristics and structures of the East Asian atmospheric circulation. It profoundly affects the outbreak and development of the Asian summer monsoon and the distribution of rain bands in eastern China (Duan and Wu, 2005; Yanai and Wu, 2006; Wang and Zeng, 2008; Liu *et al.*, 2012; Wu *et al.*, 2012a).

With the abundance of TP observation data and the development and improvement of modern models, an increasing number of studies have noted that summer precipitation in eastern China is closely related to the TP (Luo and Yanai, 1983; Wang *et al.*, 2013). The downstream transmission of Rossby wave trains generated on the TP could provide favourable conditions for triggering and developing clouds and precipitation in eastern China (Wang *et al.*, 2013; Wu *et al.*, 2016a). In addition, Xu *et al.* (2015) concluded that the TP affects the spatial and temporal evolution of precipitation in eastern China by influencing the path and intensity of water vapour transport from the low-latitude ocean to the land.

Previous authors have discussed the climatic effects of TP topography (Manabe and Terpstra, 1974; Liu and Yin, 2002; Boos and Kuang, 2010; Wu *et al.*, 2012a; Zhang *et al.*, 2015). The role of TP topography in circulation is closely related to the state of the circulation. When anomalous changes occur in individual members of the monsoon system, the role of TP topography also changes. Therefore, numerical simulations are widely used to study the climate response of TP uplift. First, Manabe and Terpstra (1974) and Kutzbach *et al.* (1989) studied the influence of TP topography on climate by using a low-resolution climate model. Based on the existing terrain, only natural terrain experiments and mountain-free experiments were carried out. The influence of large-scale TP topography on the monsoon was studied. It was concluded that the large-scale TP topography makes the middle and high latitudes of East Asia arid. Subsequently, in the early 21st century, Liu and Yin (2002) and Abe *et al.* (2003) conducted analyses by using the linear elevation increase method (in which the actual terrain elevation is multiplied by a certain percentage) to start with the removal of all terrain and gradually increase the TP terrain. They found that different terrain heights had

different effects on the intensity of the monsoon and the TP has a greater impact on the East Asian monsoon. However, previous studies were limited by computational performance, and only low-resolution data could be used to explore the influence of the TP on the monsoon as a whole. It concluded that the TP is a significant heat source in summer and that most of the TP is a cold source in winter. The different effects of cold and heat sources make the TP have different effects on the local and downstream weather, climate and atmospheric circulation (Yeh *et al.*, 1957; 1979; Yanai *et al.*, 1992). Therefore, the land-ocean interactions and block experiments are conducted on the TP (e.g., Wu *et al.*, 2012b) and it concluded that the South Asian summer monsoon (SASM) and the East Asian summer monsoon (EASM) are influenced by the TP. The ocean drive also plays an important role.

With the improvement of computational power and the physical framework of climate models, the climate effects generated by different parts of TP topography are gradually being studied at higher resolutions. The influence of the significant topographic uplift of the TP on the monsoon had been discussed in blocks, starting from removing all topography (e.g., Tang *et al.*, 2012; Zhang *et al.*, 2015; Yu *et al.*, 2018). It found that specific areas of the TP, rather than the whole TP, play a dominant role in influencing the SASM and EASM. The uplift of the TP favours precipitation downstream. Wu *et al.* (2012b) divided the water vapor transport of the SASM into two branches. For the southern branch, the sea-land thermal contrast in the Tropics causes water vapor to be concentrated in a belt and transported from the west to east along the ocean south of 20°N. Water vapor is deflected by the subtropical high to produce a northerly component, which is transported to the southeast coast of China and the Japanese islands. For the northern branch, the northward directed moisture is transported to the slopes of the TP and is lifted to produce convective clouds and intense precipitation. Arriving water vapor is transported east and northeast, bringing sufficient water vapor downstream to sustain the EASM. However, for the northern branch, the relationship between the “thermal column” on the TP and the wet flow in the Asian summer wind circulation was investigated by Xu *et al.* (2014), which found that the thermal structure of the TP leads to two dynamic processes of low convergence zone and high dispersion coupling on the southern slope of the TP and on the main terrace, which transfer the wet air to the TP through two steps. The first step is the mechanical action caused by the uplift of the southern slope of the TP, which forces water vapor to be lifted onto the TP platform. This large platform is strongly heated by solar radiation, so that the water vapor lifted to the TP continues to be lifted by thermal forces to form convective clouds,

and is transported downstream. Apart from this, the TPSA correlates with the precipitation level, distribution and convective activity in the middle-lower reaches of the Yangtze River Delta (YRD) and influences the direction of water vapor transport (Dong, 2018). Topographic forcing generated in different areas of the TP has different effects on the northern branch of the SASM. At the same time, different climatic responses to local and downstream regions are produced, which affect the EASM advance in different directions. Therefore, it is necessary to study the dynamic anomalies, thermal anomalies and regional climate responses caused by topographic forcing in different regions.

For the different regions of the TP, the differences in cloud and precipitation characteristics are prominent. The cloud water content in the southeastern TP is obviously higher than that in the northeastern TP, while the cloud water content in the eastern Tibetan Plateau (ETP) is higher than that in the western TP (Wang *et al.*, 2015). Precipitation and convective activity frequency in the southeastern TP are more abundant than those in other parts of the TP (Zhao *et al.*, 2018). In the southeastern TP, the moisture sources are mainly from the transport of Indian monsoons, with obvious upward vertical motion and abundant heat and moisture, while in the northeastern TP and western TP, the moisture and heat sources are relatively poor (Chen *et al.*, 2019; Li *et al.*, 2020). ETP is also an important contributing region to convective clouds and precipitation in the YRD. Southern East China (SEC) and Central East China (CEC) are influenced by the advance of ESAM to different degrees. In contrast, the CEC is an area of flat topography in the YRD that is meteorologically famous for the Meiyu period during early summer, which is a distinct seasonal characteristic for this region. Zhao (2016) found that the eastward shift of the water vapor transport power system on the TP affects mainly the CEC. However, Wei *et al.* (2015) indicated through diagnostic analysis that the location of South Asian High (SAH) has different effects on precipitation in the YRD. The southeast (northwest) movement of the SAH leads to an increase (decrease) in precipitation in the CEC and a decrease (increase) in precipitation in the SEC. Thus, different regions of the TP can influence the intensity and location of SAH, which may lead to changes in the location of precipitation zones and precipitation characteristics in the downstream areas of the TP. These regions experience different circulation patterns and moisture conditions, and they exhibit different cloud and precipitation conditions. Therefore, the analysis of these regions under different topographic conditions is of interest.

In this work, sensitivity experiments on the regional uplift of the TP were conducted using the Weather

Research and Forecasting (WRF) model with a horizontal grid spacing of 27 km. The mechanism driving changes in Asian monsoon dynamics and cloud microphysics caused by topographic uplift in different regions of the TP were studied. The individual and overall roles of the North Branch of the SASM and EASM in advancing downstream due to different topographic components were systematically evaluated. For these reasons, we investigate the changes in the northern branch of the SASM caused by regional topographic uplift and the physical factors and dynamic mechanisms of water vapor transport and precipitation in the ETP, CEC and SEC. Section 2 of this study presents the data, model and analysis methods used in this research. Section 3.1 provides an evaluation of the model results. Sections 3.2–3.5 analyse and discuss the issues raised through the spatial differences and correlation analyses of each experiment's dynamics and physical quantities at different heights and vertical directions.

2 | DATASETS AND MODEL CONFIGURATION

2.1 | Data

In this research, precipitation data were obtained from the China National Meteorological Information Centre (<http://data.cma.cn/>), which combines precipitation data from Chinese automatic stations with precipitation data retrieved by the Climate Prediction Center Morphing Technique (CMORPH) (Pan *et al.*, 2012; Yu *et al.*, 2013; Zhang and Jiang, 2013; Shen *et al.*, 2014). The warm-season precipitation dataset for from June to September 2011–2020, which is obtained by combining ground observation data and CMORPH satellite data, is used in this study. The hourly precipitation data of more than 30,000 automatic observation stations in China are used as the ground observation field, and the real-time satellite inversion CMORPH precipitation data of the National Centers for Environmental Prediction (NCEP) are used as the background field. The hourly products on regular latitude-longitude grids at $0.1^\circ \times 0.1^\circ$ are obtained through the optimization of spatial distribution and error characteristics and through quantitative evaluation and analysis in the range of $70^\circ\text{--}140^\circ\text{E}$, $15^\circ\text{--}59^\circ\text{N}$.

The reanalysis data used in this study were obtained from the European Centre for Medium-Range Weather Forecast (ECMWF), which regularly uses its prediction model and data assimilation system to reanalyse archived observations to create an ERA5 hourly global dataset describing atmospheric, terrestrial and marine changes from 1979 to the present (Hersbach *et al.*, 2020). In this

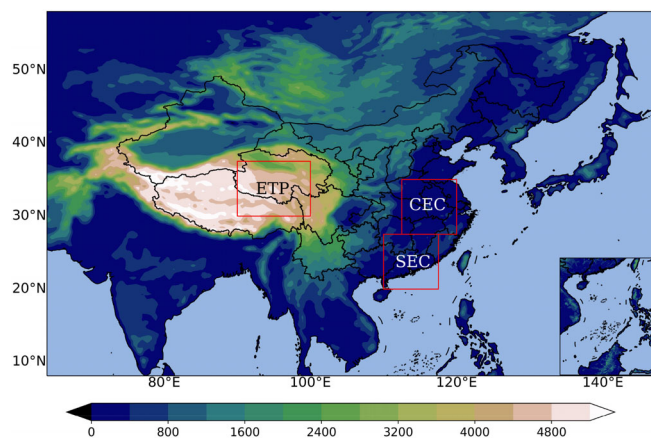


FIGURE 1 Topography (m) of the WRF domain and the selected regions: SEC, CEC, and ETP (marked with boxes)

work, the period used is from June to September of each year from 2011 to 2020. Data were obtained for estimates of atmospheric variables at a horizontal resolution of $0.25^\circ \times 0.25^\circ$ with a total of 37 layers in the vertical direction (from 1,000 to 1 hPa).

2.2 | Model description and experimental design

The study employed the mesoscale WRF model (v4.2), which was developed by the National Centre Atmospheric Research (NCAR), the National Oceanic and Atmospheric Administration (NOAA) and other partners (Skamarock *et al.*, 2019). The model uses a terrain-following coordinate system with a horizontal Arakawa-C grid and a three-order Runge–Kutta time integration scheme. Previous studies have shown that the WRF model can well reproduce the observed climatic characteristics in the current simulation and has potential for predictive simulations of East Asia (Yu *et al.*, 2014; Park *et al.*, 2015; Wang *et al.*, 2020).

Initial and boundary conditions were derived from the ERA5 reanalysis dataset with $0.25^\circ \times 0.25^\circ$ spatial resolution and 6-hr temporal resolution (00:00, 06:00, 12:00 and 18:00 UTC). The simulation area has a spatial resolution of 27 km and grid points of 275×211 . The centre point is located at 105.48°E , 37°N . The simulation domain is shown in Figure 1. In the vertical direction, the model has 32 eta levels with a top level of 50 hPa. The output interval is hourly, and the integration time is 920 days, from 00:00 on June 1 to 00:00 on September 1 (UTC) each year from 2011 to 2020. The first 2 days are used as the spin-up time of the model, and the hourly simulation results for 90 days per year are selected as the effective simulation results for analysis (total of

TABLE 1 WRF model setup

Simulation area number	d01
Simulation period	From 2011 to 2020, June 1 to September 1
Time step	108 s
Map projection	Mercator conformal conic
Vertical levels	32 eta levels
Model top	50 hPa
Meteorological input data	ERA5 6-hr reanalysis data ($0.25^\circ \times 0.25^\circ$)
Horizontal grid spacing	27 km (275×211 grid points)
Microphysics	WSM6-class scheme (Hong and Lim, 2006)
Longwave radiation	RRTMG scheme (Iacono <i>et al.</i> , 2008)
Shortwave radiation	RRTMG scheme (Iacono <i>et al.</i> , 2008)
Surface layer	MM5 scheme (Skamarock <i>et al.</i> , 2008)
Land surface model	Unified Noah land surface model (Tewari <i>et al.</i> , 2004)
Cumulus convective	Kain-Fritsch scheme (Kain, 2004)
Planetary boundary layer	Yonsei University scheme (Hong <i>et al.</i> , 2006)

900 days). This strategy prevents the model from deviating too far from the forcing data. The model setup is summarized in Table 1. Only the topography was changed in these sensitive experiments, and other physical boundary conditions, such as the underlying surface type, soil characteristics and land–sea distribution, remained unchanged. The specific settings of the five groups of experiments are shown in Figure 2.

Con1: The experiment makes use of the original topography and serves as a reference to understand the influence of topographic modifications in other experiments.

Con2: Retains the TP area and set the elevation of the other areas to 1 m. The purpose of removing terrain other than the TP is to remove the effect of drag forces generated by small terrain on the experiment. James and Houze (2005) pointed out that the influence of topography on precipitation is a multiscale process, and topography can affect the development of large-scale troughs and ridges the oblique pressure of the atmospheric field of mesoscale air masses and the development of small-scale convective processes.

Con3: Retains the TP area, set the elevation of the other areas to 1 m and removes sensitive areas of the TP. We define the southeast edge of the TP ($98^\circ\text{--}105^\circ\text{E}$,

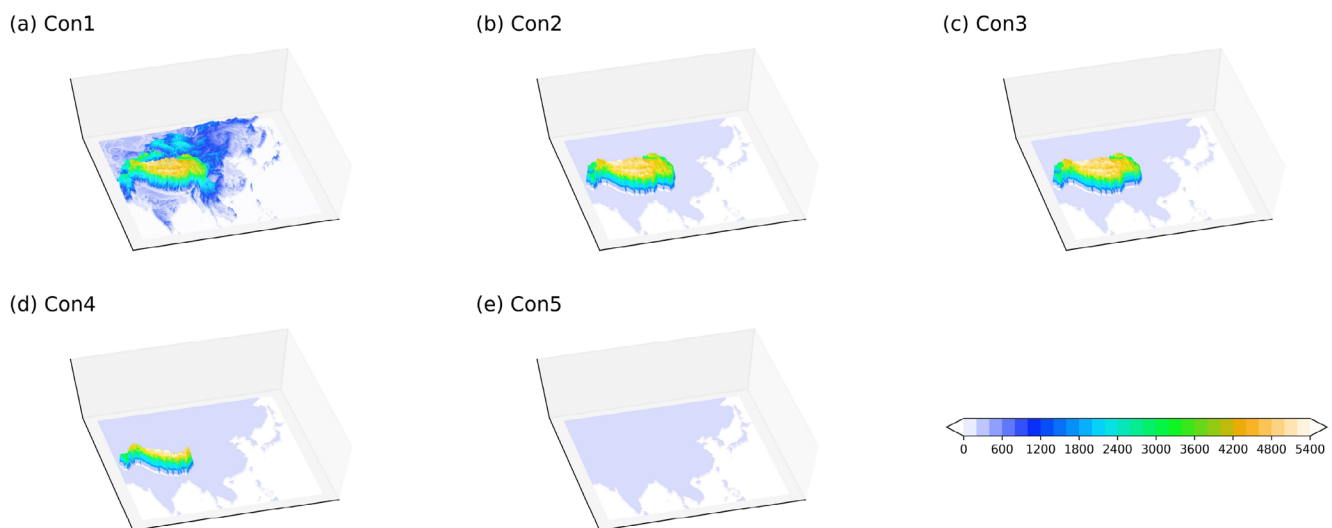


FIGURE 2 Topographic distribution of sensitivity experiments (m)

25°–32.5°N) as the TP sensitive area (referred to as the TPSA), where the topography is gently undulating compared to the southern slope of the TP, making it easier for water vapor to climb. It is also a unique trumpet topography, which is conducive to the convergence and transport of water vapor. Dong (2018) found that the TPSA correlates with the precipitation level, distribution and convective activity in the YRD and influences the direction of water vapor transport. After removing the TPSA, the effect of the TPSA on different areas of the YRD is explored.

Con4: Same as Con3 but remove the middle and rear parts of the TP. We know that the TP has steep slopes and that the surface rises sharply on its southern and eastern edges. However, on the plateau, the TP extends widely to the north and west in a relatively flat manner. Thus, it appears as a very large platform that is strongly heated by solar radiation. The water vapor that has climbed to the TP continues to lift, generating strong convection. The experiment is used to investigate the respective roles of the TP south slope and the TP platform.

Con5: Set all terrain to 1 m. This is the same as Con4 but remove the southern slope of the TP. Only the influence of sea–land interaction on the experiment is considered. The details of the experiments are shown in Table 2.

2.3 | Analysis methods

To investigate the relationship between moisture flux and precipitation, the vertical integral of the water vapor flux (IVT) from 1,000 to 300 hPa was used to describe the water vapor transport characteristics (Martin *et al.*, 2004; Neiman *et al.*, 2008; Cordeira *et al.*, 2013),

TABLE 2 Experimental design

Experiment	Description
Con1	Control experiment: Real terrain
Con2	Retain TP area, set the elevation of other areas to 1 m
Con3	Retain TP area, set the elevation of other areas to 1 m and remove sensitive areas of the TP
Con4	Same as Con3 but remove the middle and rear parts of the TP
Con5	Set all terrain to 1 m

$$\text{IVT}_u = -\frac{1}{g} \int_{1,000}^{300} q u dp,$$

$$\text{IVT}_v = -\frac{1}{g} \int_{1,000}^{300} q v dp,$$

$$\text{IVT} = \sqrt{\text{IVT}_u^2 + \text{IVT}_v^2},$$

where IVT_u and IVT_v ($\text{kg}\cdot\text{m}^{-1}\cdot\text{s}^{-1}$) are the zonal and meridional components of the IVT, respectively; u and v ($\text{m}\cdot\text{s}^{-1}$) are the layer-averaged zonal and meridional wind speeds, respectively; g ($\text{m}\cdot\text{s}^{-2}$) is the acceleration of gravity; q ($\text{kg}\cdot\text{kg}^{-1}$) is the layer-averaged specific humidity; and dp is the pressure difference between two adjacent pressure levels. Eastward (northward) IVT_u (IVT_v) is defined as positive.

To explore the interaction between the water cycle process and monsoon activity, the correlation vector method is used to analyse the precipitation series and

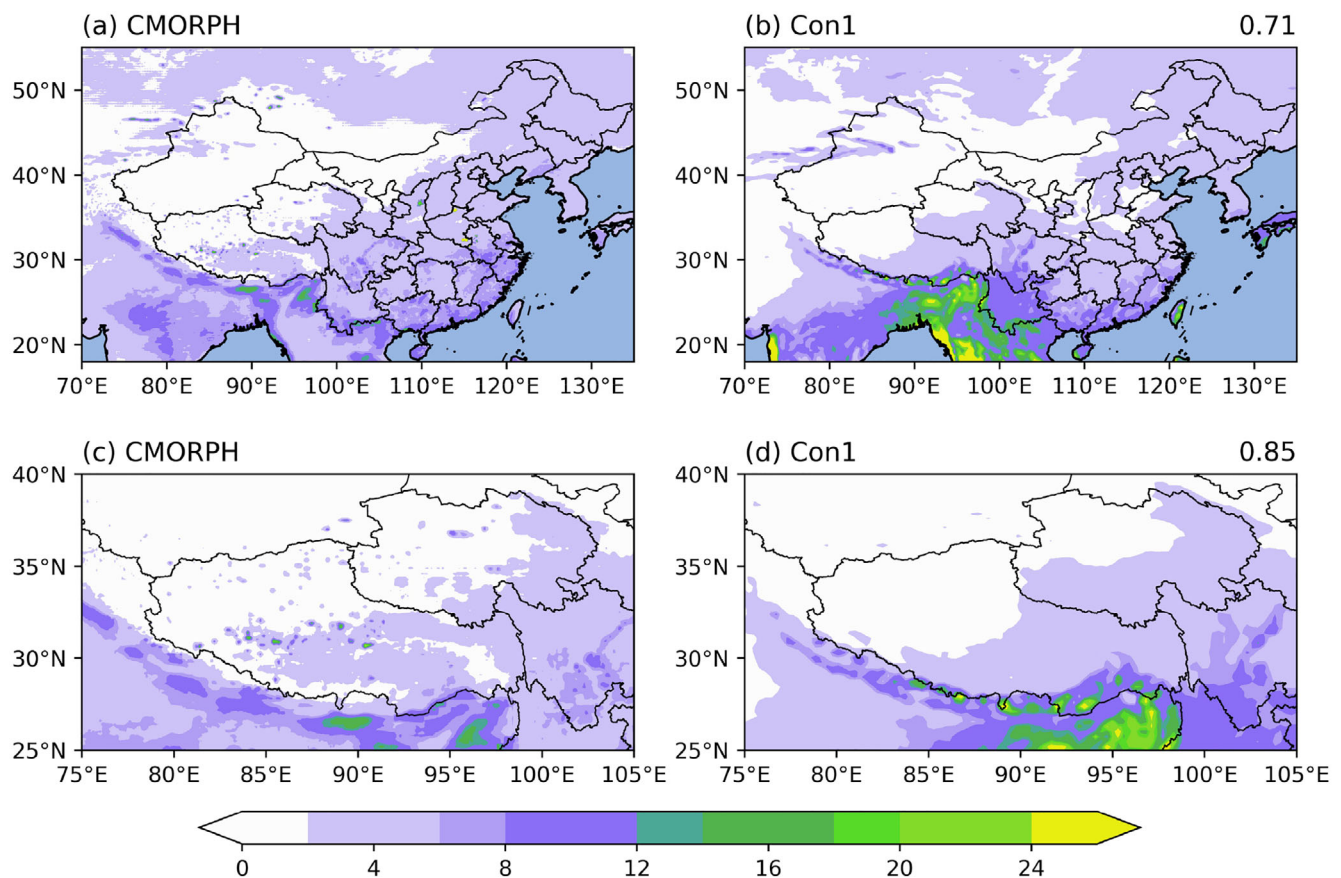


FIGURE 3 Spatial distribution of daily average precipitation for CMORPH (a, c) and Con1 (b, d) from 2011 to 2020 ($\text{mm} \cdot \text{day}^{-1}$); panels (a, b) for East Asia; panels (c, d) for the TP. The spatial correlation coefficients between CMORPH and Con1 are labelled in the upper right corner

IVT (e.g., Bai and Xu, 2004; Miao *et al.*, 2004). The current research uses this method to track the influence of different TP terrain heights on the summer water vapor transport trajectory in the YRD.

To characterize the correlation between the daily average precipitation and IVT, the correlation coefficient was tested by table lookup. If the significance level was better than $\alpha = 0.01$, the correlation coefficient was considered significant,

$$R = \frac{\sum_{i=1}^N (O_i - \bar{O})(p_i - \bar{p})}{\sqrt{\sum_{i=1}^N (O_i - \bar{O})^2} \sqrt{\sum_{i=1}^N (p_i - \bar{p})^2}}$$

3 | RESULTS

3.1 | WRF performance

The model performance was evaluated by comparing the simulation results to the hourly precipitation data from

the CMORPH. To better compare the simulated and CMORPH precipitation data, the CMORPH were interpolated into the grid of the model results for comparison. The model results and CMORPH daily average precipitation data were studied from 2011 to 2020.

The precipitation distribution of the CMORPH was similar to ground observation results, and they had a reasonable correlation (Zhao, 2018), which is basically in line with the spatial distribution characteristics of precipitation in China. Therefore, the spatial distribution characteristics of summer precipitation were described by the CMORPH (Figure 3a). The southeast coast has more precipitation than the inland area, and the precipitation decreases from east to west. The precipitation is less than $2 \text{ mm} \cdot \text{day}^{-1}$ in northwest China, and the precipitation is in the range of $6\text{--}10 \text{ mm} \cdot \text{day}^{-1}$ in east China, which is consistent with the results of Xu *et al.* (2013). Comparing the CMORPH, the WRF model can capture the spatial distribution characteristics of precipitation well in East Asia, and the spatial correlation coefficient is 0.71 (Figure 3a,b). Compared with the results of Liu and Yin (2002), who used CAM4 to simulate East Asian precipitation, the results of this model are superior. However,

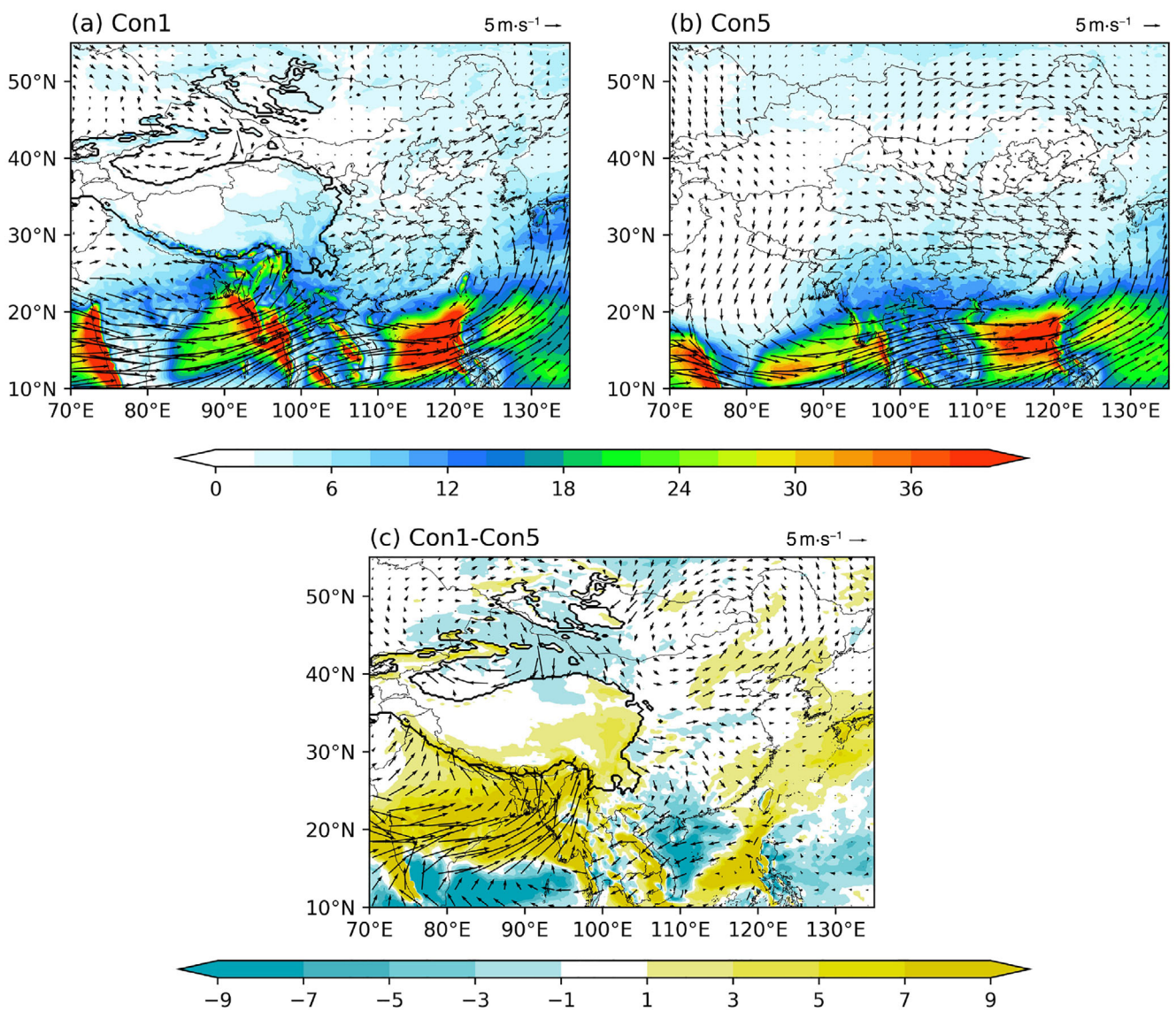


FIGURE 4 Average daily precipitation ($\text{mm} \cdot \text{day}^{-1}$) and 850 hPa circulation ($\text{m} \cdot \text{s}^{-1}$) of Con1 (a) and Con5 (b), labelled as $5 \text{ m} \cdot \text{s}^{-1}$; (c) difference between average daily precipitation and 850 hPa circulation ($\text{m} \cdot \text{s}^{-1}$) of Con1 and Con5 ($\text{mm} \cdot \text{day}^{-1}$). The black line is the 2,000 m altitude contour line

there are excessive precipitation bias in Myanmar and Thailand in Con1, which is a common drawback of numerical models for setting sea surface temperatures (Cavazos *et al.*, 2019; Ashfaq, 2020).

The model results show that the distribution of summer precipitation decreases from southeast to northwest on the TP (Figure 3c,d), which agrees with the CMORPH dataset. Along the Himalayas, there is a clear topographically driven precipitation maximum. The northern section of precipitation moves along the Himalayas to the TPSA. The spatial correlation coefficient of the CMORPH and model results reaches 0.85, and the model results accurately simulate the spatial distribution of summer precipitation on the TP. However, the simulated precipitation in the southern part of the TPSA exhibits an

overestimation bias, which is similar to the results of previous studies (e.g., Wu *et al.*, 2016b; Liu *et al.*, 2017).

In summary, the WRF model can reproduce the observed precipitation characteristics in East Asia. Therefore, based on this model setting, we conducted sensitivity experiments.

3.2 | Topographic influence on lower levels

In Con1, the effects of land-sea thermal forcing create centres of intense precipitation along 15°N in East Asia (Figure 4a). The SASM separates the coastal plains of southwestern India and Myanmar from the inland basins

in the mountains and along the Himalayas, showing clear topographically driven precipitation. There is a cyclonic system in the low level of the SAH in northern India (25° – 30° N). The northern branch of the SASM transports water vapor to the TP along the north. The water vapor hardly rises to the TP due to the topography blocking the lower wind field producing bypass flow. The northern part of the precipitation moves along the Himalayas to the TPSA. The prevailing westerly winds under subtropical high carried large amounts of water vapor to the East Asian continent, producing abundant precipitation in eastern China and East Asia.

Con5 eliminates all topographic forcing and retains sea–land thermal forcing. Precipitation areas are mainly concentrated south of 20° N (Figure 4b). Heavy precipitation centres are still present in western India, the Bay of Bengal and the South China Sea. The topography-driven precipitation disappears in the western high elevations. Due to the elimination of the topography, the cyclonic nature of the SAH at low altitude disappears at low altitudes, and the northern branch of the SASM disappears. As a result, it leads to the enhancement of the southern branch of the SASM, and precipitation at low latitudes shows positive anomalies. At mid-latitudes, the precipitation in central and northern China shows negative anomalies, and the airflow is transported to the northeast. The differences in daily mean precipitation and 850 hPa circulation between Con1 and Con5 show that topography has a strong influence on circulation and precipitation (Figure 4c). Forced by the topography of the TP, low-level circulation conditions produce a bypass. In the YRD, precipitation is reduced by low-humidity winds and low-latitude ocean transport along the TP bypass. This result is similar to those previously reported (Wu *et al.*, 2012b; Zhang *et al.*, 2015).

The differences in the daily mean precipitation and 850 hPa circulation between the experiments are explored (Figure 5). The anticyclone appears in northern Xinjiang, and the cyclone is strengthened in northern China. Both cyclones and anticyclones intensify with the elimination of topography in the mid-latitudes. The removal of topography except the TP causes local effects and the disappearance of drag. The airflow through the TPSA is transported from the TP to the east of China (Figure 5a). Water vapor is predominantly bypassed in the lower layers. Less water vapour is lifted by the climbing flow, resulting in less precipitation on the southern slope of the TP. More water vapor is transported from the southeastern part of the TP to the YRD. The precipitation is concentrated at low latitudes. After removing the TPSA, the SEC precipitation increases, while that the CEC is almost unchanged (Figure 5b). This may be due to the effect of the TPSA on the direction of bypassing

water vapor, which deflects water vapor toward SEC. When only the southern slope of TP is available, it leads to a weakening of water vapor uplift in the TP platform, which directly leads to the disappearance of precipitation in ETP (Figure 5c). When only the role of the platform is considered (Figure 5d), the platform plays a dominant role in precipitation in the ETP. At the same time, it has a blocking effect on the southward flow of dry and cold air at mid-latitudes. He (2012) explained that the southward slope of the TP is an important factor in generating and maintaining the SASM without considering the sea–land thermal differences. It leads to the enhancement of the northern branch of the SASM. If only the role of the southward slope is considered (Figure 5e), the southward slope of the TP has a strengthening effect on the SAH, thus enhancing the northern branch of the SASM. The anomalous dry and cold flow from the north southward converges with the northern branch of SASM causing anomalous precipitation near the Bay of Bengal. Based on the average daily precipitation at each regional grid point, the ETP precipitation decreases and shifts southward after removing the regional topography (Figure 5). Most of China has negative precipitation anomalies. There is little change in precipitation in CEC and a slight increase in precipitation in SEC.

In summary, the topographic uplift of the TP in summer produces an excitation effect in East Asia. In the topographic sensitivity removal experiment, the generation and development of low-level cyclonic high disturbances in South Asia influenced by topography are suppressed. In contrast, removal of topography in mid-latitudes favours the generation and development of mid-latitude cyclones and anticyclones. The existence of the platform on the TP is beneficial to local precipitation and prevent the mixing of dry and cold air in the mid-latitude, warm and humid air in the low latitude. The existence of the southern slope facilitates the maintenance and development of the SAH and mid-latitude anomalous circulation. The precipitation belt shifts southward, and there is a tendency to reduce precipitation over most of China. The presence of the TP enhances the SAH so that the precipitation in northern India and the Bay of Bengal shows positive anomalies. Condensation heating in the precipitation centre generates SAH low-level cyclonic circulation in the lower layer and further strengthens the SASM, which implies positive feedback between precipitation and circulation.

3.3 | Topographic influence on middle levels

The TP has an essential influence on the formation and development of atmospheric circulation, climate change

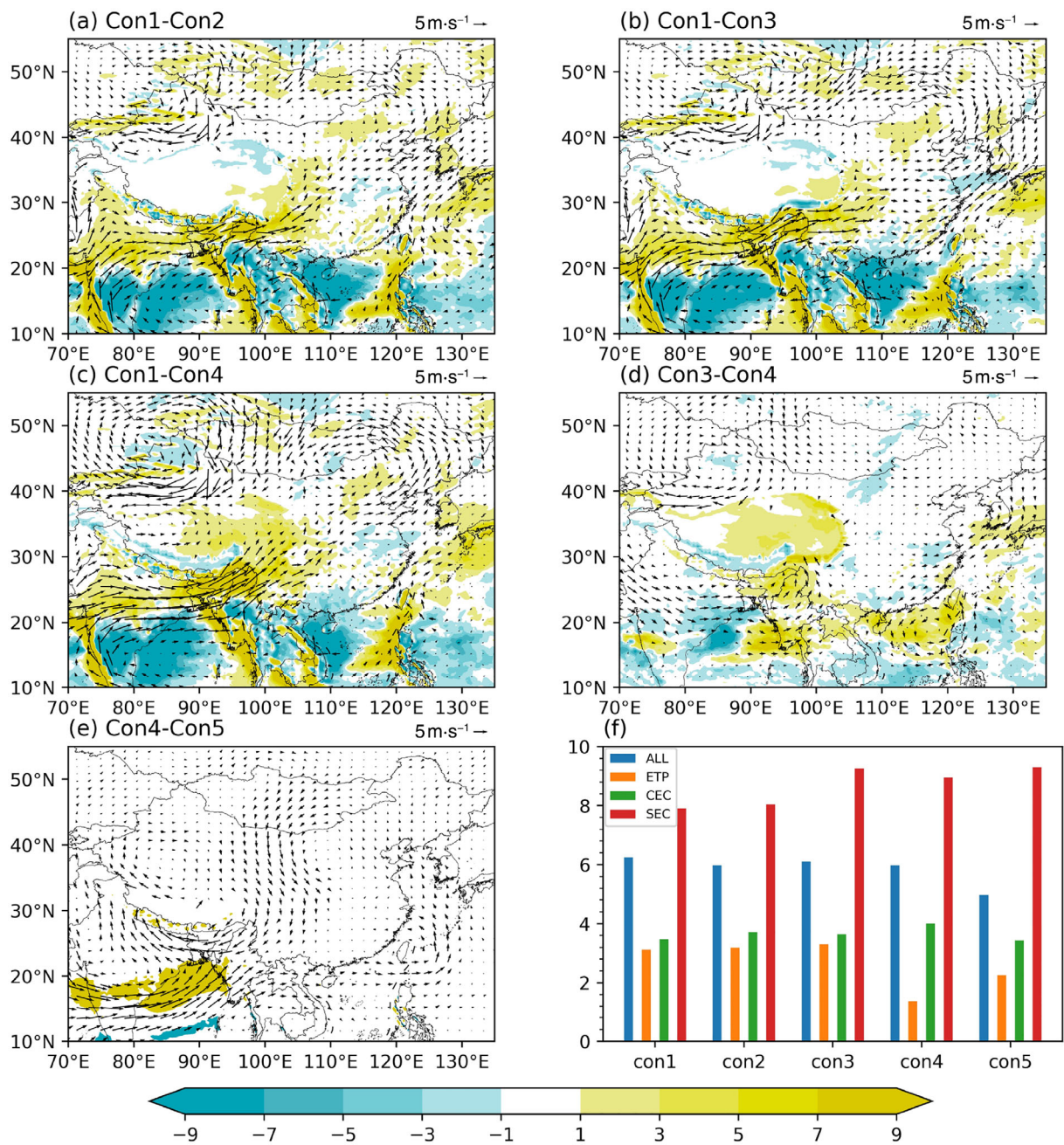


FIGURE 5 Difference between the average daily precipitation ($\text{mm} \cdot \text{day}^{-1}$) and 850 hPa circulation ($\text{m} \cdot \text{s}^{-1}$). Con1-Con2 (a), Con1-Con3 (b), Con1-Con4 (c), Con3-Con4 (d), Con4-Con5 (e), average daily precipitation for each regional grid point (f) ($\text{mm} \cdot \text{day}^{-1}$)

and catastrophic weather in East Asia (Yeh *et al.*, 1979; Duan and Wu, 2005; Liu *et al.*, 2012). The water vapor transported from low latitudes can rise to the TP at 500 hPa (e.g., Ding, 1993; Sun and Zhang, 2012). The convective clouds generated by the water vapor climbing to TP will propagate eastward and enhance the precipitation in the YRD.

To further explore the effects of topographic changes on the circulation and convective clouds, the spatial distribution of convective clouds and 500 hPa circulation

are further analysed (Figure 6). The spatial distribution of convective clouds and precipitation in Con1 is similar (Figure 4a), and SASM places the mountains of southwest India and Myanmar and along the Himalayas showing clear topography-driven uplift-generated convective clouds (Figure 6a). At the same latitude, the distribution of convective clouds is lower in the eastern part of the TP than in the western part. Convection is strong, and precipitation is also substantial. The conclusions drawn here are similar to those of Kang and Gong (2021).

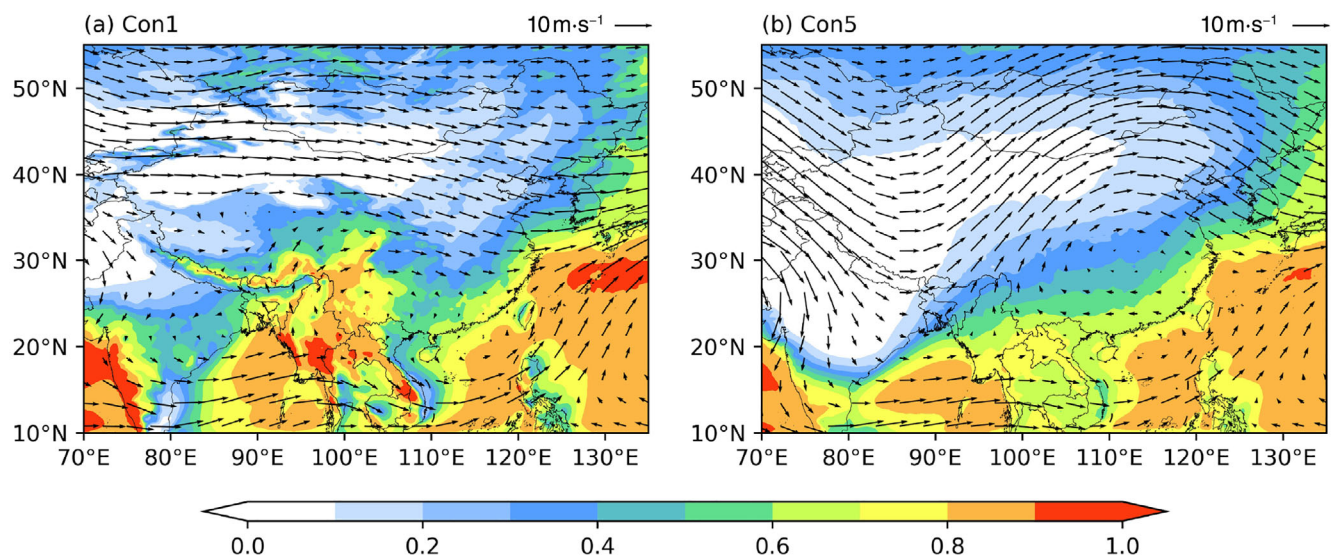


FIGURE 6 Average convective cloud cover and 500 hPa circulation ($\text{m}\cdot\text{s}^{-1}$) of Con1 (a) and Con5 (b), labelled as $10 \text{ m}\cdot\text{s}^{-1}$

Convective clouds are concentrated from the low-latitude ocean to the Bay of Bengal, Thailand and TP. The extension of water vapor from the low-latitude ocean and lifting into the TP constitute a large monsoonal water vapor transport triangle at 500 hPa, as found by Xu *et al.* (2002). In the background of low-latitude oceanic water vapor transport, convective clouds caused by significant uplift of important topographic features are concentrated at 500 hPa. The northern branch of SASM deflects to the TP under the influence of the SAH, while the prevailing westerly winds in the mid-latitudes also transport water vapor to the TP. The main structure of SAH is thought to be high-altitude divergence and low-altitude convergence (Mason and Anderson, 1963; Krishnamurti *et al.*, 1973). The SAH maintains a high water vapor column on the TP through the transport of water vapor to higher altitudes and the evaporation of water vapor from the surface. Therefore, convective cloud concentration zones exist on the southern slope of the TP and the front of the TPSA. The spatial distribution of precipitation in this finding (Figure 4) is similar. Xu *et al.* (2019) suggested that the water tower effect would result in water vapor being transported to higher altitudes, and the latent heat release from condensation then increases. As heat from water vapor rises, a large amount of supercooled cloud water in the air forms clouds. Water vapor further condenses to release latent heat to heat the atmosphere. This process is accompanied by westerly transport, so convective clouds on the TP are concentrated in ETP. However, convective clouds, which are delivered to CEC, are produced northward by the low-latitude trans-mountain warm and humid airflow entering from the TP. The merging is transported by the

prevailing mid-latitude westerly winds merging around the airflow. In contrast, convective clouds in SEC are mostly contributed by low-latitude oceanic high-humidity flow. Therefore, the convective clouds in SEC are more numerous than those in CEC.

In Con5, with all topography removed, there is a distinct trough ridge north of 30°N at 500 hPa (Figure 6b). The low-pressure trough is controlled near 48°N, 85°E, and the high-pressure ridge in northeast China is controlled at 120°E. The spatial distribution of convective clouds in East Asia is based on the characteristics of the trough-ridge distribution. The prevailing westerly winds in the mid-latitudes are influenced under the influence of a low-pressure trough, and a solid southerly component in northern India moves the SASM southward. The low-latitude warm and humid airflow compensates northwestward under the western Pacific subtropical high and joins the high-pressure ridge. The airflow is transported to CEC and the Sea of Japan. Chiodi and Harrison (2010) found that in addition to the Antarctic and Arctic, the intertropical convergence zone (ITCZ) is a large area of intense convection, located near 12°–15°N in summer. This causes the low-latitude oceans to become an area of convective cloud concentration. Due in part to circulation, the eastward convective cloud masses originating from the TP disappear in Con5. Convective clouds are mainly transported by low-latitude oceanic movement.

The difference in the convective cloud amount and 500 hPa circulation between the experiments are shown in Figure 7. Overall, the removal of topographic factors reduces convective clouds in the TP, south slope and TP downstream compared to the control experiment and

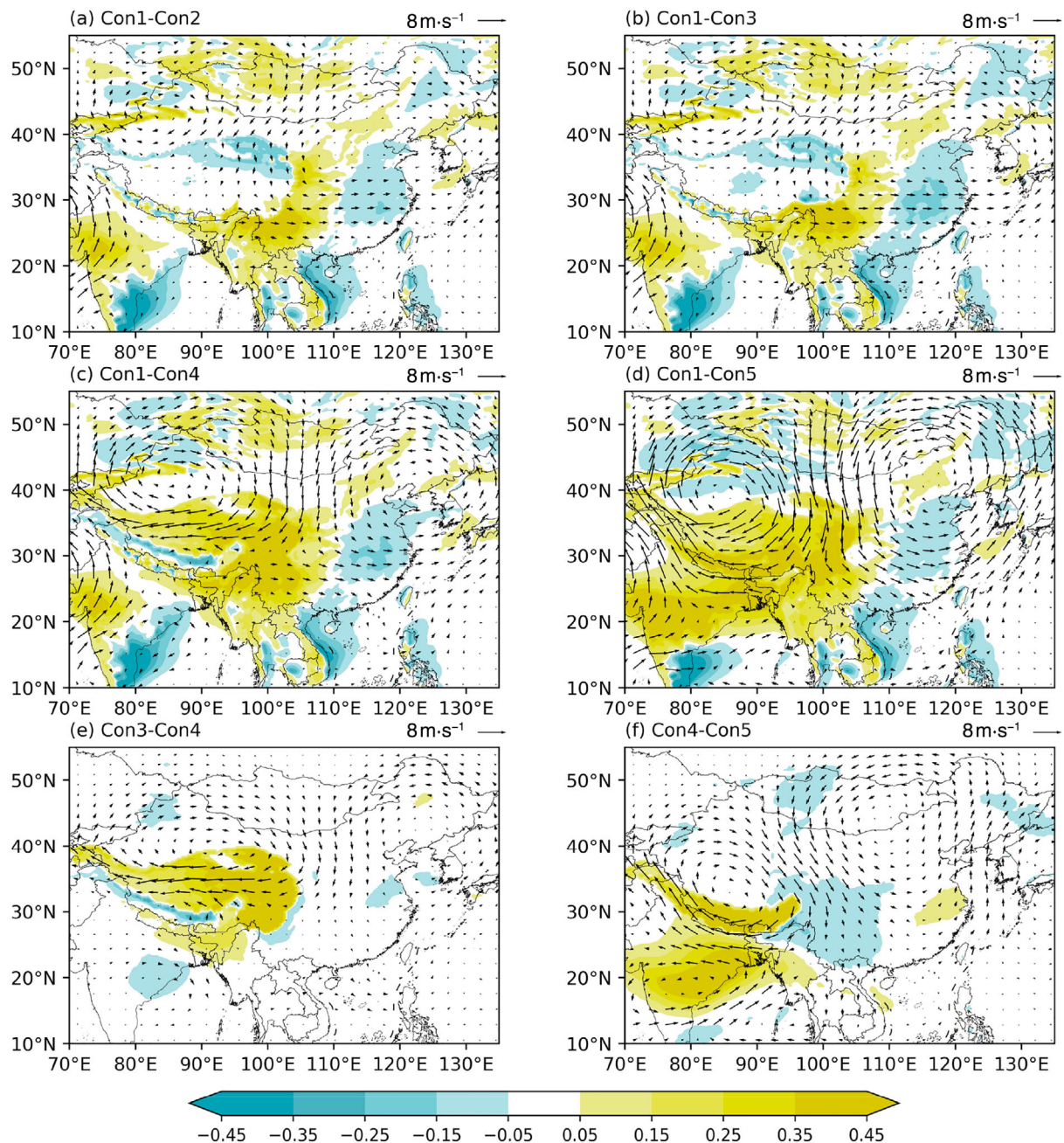


FIGURE 7 Difference between the convective cloud cover and 500 hPa circulation ($\text{m}\cdot\text{s}^{-1}$). Con1-Con2 (a), Con1-Con3 (b), Con1-Con4 (c), Con1-Con5 (d), Con3-Con4 (e), Con4-Con5 (f)

increases convective clouds in the YRD. The southward component of the prevailing westerly winds is enhanced at mid-latitudes due to the absence of topographic barriers beyond the TP (Figure 7a). The southward shift of the SASM reduces the transport of warm and humid air flow from northern India and increases the moisture from southern India. As a result, the moisture in the TP decreases, and convective clouds decrease in the ETP and its downstream. With the removal of TPSA (Figure 7b), the convective clouds in the SEC region show positive anomalies. The anticyclonic pattern in northern Xinjiang

is evident, and the cyclonic pattern in northeastern China is in confrontation with the subtropical high (Figure 7c). After removing the TP platform, the TP water tower effect disappears, and the amount of convective clouds generated by uplift decreases. The shunting effect of the TP on the mid-latitude westerly belt is weakened, and the cyclonic effect is significantly strengthened. After removing all topography (Figure 7d), convective clouds due to terrain uplift completely disappear and cyclones and anticyclones are more intensified than in other experiments. When considering only the role of the TP

platform, convective clouds are mainly concentrated platform uplift generated on the TP platform (Figure 7e). For the southern slope of TP, it is favourable for the maintenance and development of SAH to generate convective cloud concentration in central India (Figure 7f). It also favours the development of the mid-latitude circulation. In each experiment with the removal of topography, although the convective clouds transported eastward by the TP decrease, the strengthening of circulation enhances the transport of oceanic convective clouds to SEC, which increases the convective clouds in the YRD.

In summary, the significant TP topography promotes the formation of clouds by moisture currents under the influence of topography and the unique water tower effect of the TP, which facilitates the formation of convective clouds. Yeh (1950) found that the TP forms a branch of the prevailing westerly wind belt at mid-latitudes, forming two strong north-south bypass currents, consolidating, and strengthening the eastward transport of the ETP. Therefore, the presence of TP topography facilitates the transport of TP convective clouds to the YRD. Considering section 3.2, the spatial distribution of daily precipitation after the removal of topography is similar to that of convective clouds across China. With the removal of topography, it is beneficial to the generation and development of anomalous cyclones and anomalous anticyclones in the mid-latitudes, and the anomalous circulation system at the upper level is more obvious than that at the bottom, which in turn affects the weather situation in East Asia.

3.4 | Topographic influence on high-level and vertical circulation

The topographic heating effect of the TP can directly or indirectly affect the middle and upper troposphere due to its high-altitude characteristics. Therefore, the thermal forcing effect of the TP topography not only affects the monsoon circulation and precipitation in the middle and lower troposphere, but also inevitably affects the circulation situation and temperature field structure in the upper troposphere. According to Con1, a strong anticyclonic circulation (SAH) with the centre located over the front of the southern slope of the TP (28°N , 94°E) is manifested over the TP in summer, corresponding to a significant warm centre in the mass-weighted vertical mean temperature field (Figure 8). The strong heating over the TP propagates eastward along the westerly rapids that act as wave-guides and eastward to the eastern North Pacific.

When the topography other than that of the TP and TPSA are removed (Figure 9a,b), it is obvious that weakening occurs in the warm centre of the TP, while

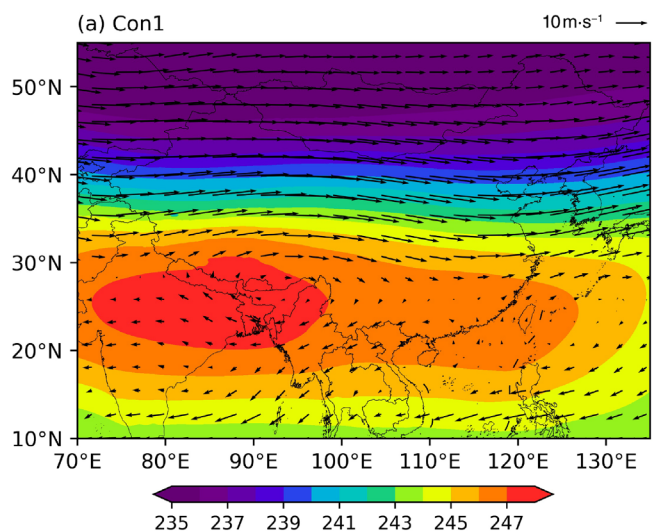


FIGURE 8 Mass-weighted vertical mean temperature (K) and circulation ($\text{m} \cdot \text{s}^{-1}$), labelled as $10 \text{ m} \cdot \text{s}^{-1}$

enhancement occurs in the cold centre in the northeastern part of the country. In the case of removing small topography, the monsoon circulation is enhanced. In combination with Figures 5 and 7, summer winds are usually accompanied by widespread convective precipitation and strong latent heat release from condensation. On the one hand, the latent heat release of condensation can heat up the middle and upper atmosphere through vertical convective motion and increase the temperature difference between sea and land. On the other hand, the phase change process can store and redistribute the solar radiation received in the Tropics and subtropics, and release it in specific regions, thus making the location and intensity of rainbands change. Thus, it greatly limits the tropospheric warming caused by precipitation in the north. When only the role of the TP platform is considered (Figure 9c,e), the warm centre is significantly weakened. Topographic heating of the TP makes an important contribution to the warming of the upper layers and maintains the position of the warm centre over the TP. The heating effect of the TP platform corresponds to the cyclonic circulation anomaly, suggesting that it has an enhanced effect on the SAH. The heating of the TP platform is more widely expressed in the upper levels, covering the whole TP, and is also more intense than the heating of the southern slope of the TP (Figure 9d,f). The southern slope of the TP makes great contributions to the circulation in the upper layers. When only the effect of the southern slope is considered, the southern slope makes the upper-level warm centre move southward and weaken. The anomalous anticyclonic cold centre appears in northeast China, which promotes the advance of the

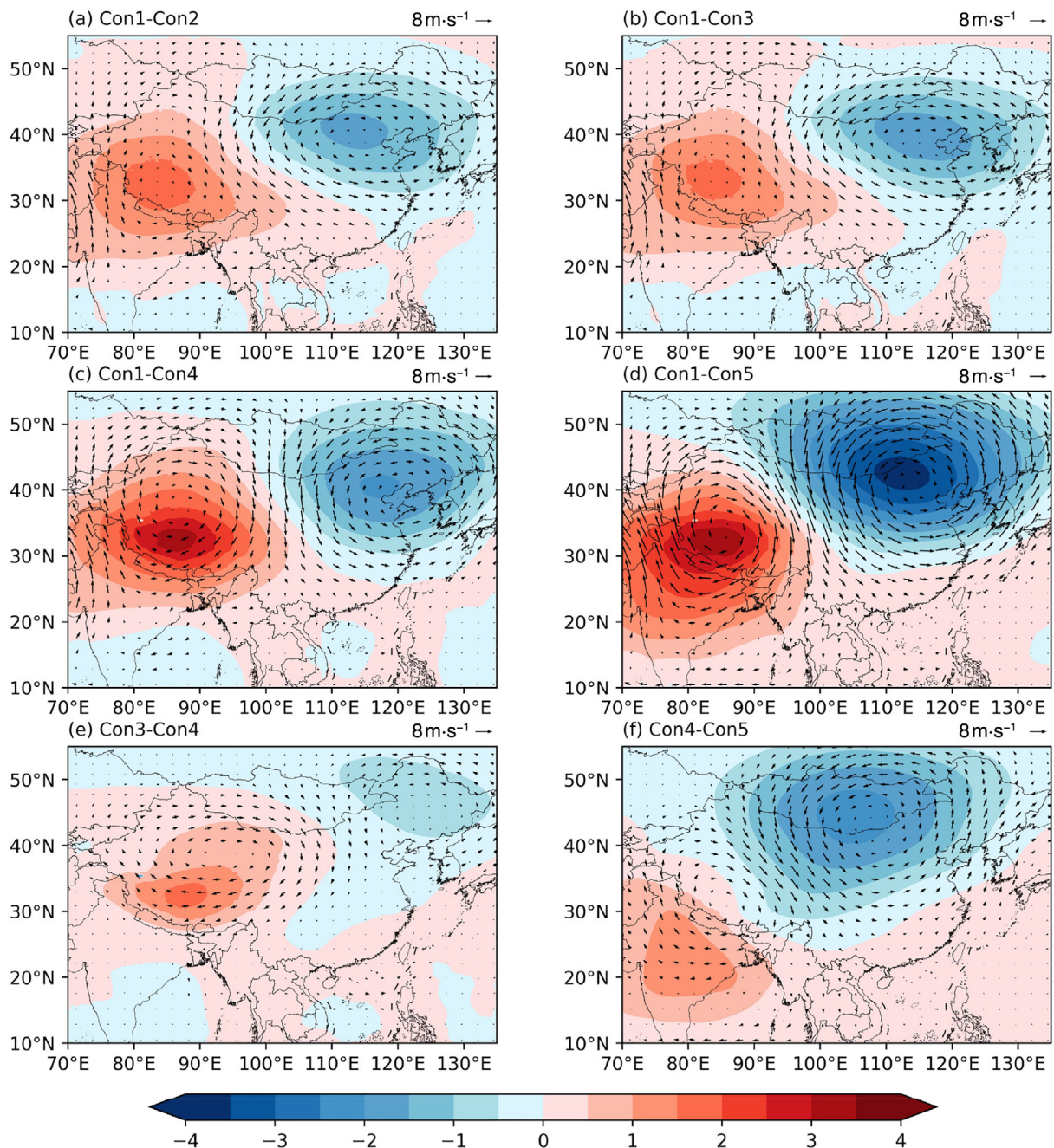


FIGURE 9 Different between the mass-weighted vertical mean temperature (K) and circulation ($\text{m}\cdot\text{s}^{-1}$). Con1-Con2 (a), Con1-Con3 (b), Con1-Con4 (c), Con1-Con5 (d), Con3-Con4 (e), Con4-Con5 (f)

EASM. At the same time, the south slope has a warming effect on the upper layers of the SAH. This is similar to previous findings that thermal forcing of the TP platform and the southern slope can excite large-scale fluctuations and propagate downstream (Wang *et al.*, 2008; Wang *et al.*, 2013). However, except for the southern slope of the TP, the heating of the TP platform make important contributions to the strengthening of the high-level warm centre of the SAH. Because of the large extent and intensity of TP heating, this may allow topographic heating of

the TP to affect sea–land thermal differences as well as meridional circulation on a larger scale. In addition, when the entire TP topography is removed (Figure 9d), the effect on the upper levels is more pronounced, with the warm centre of the upper levels cooled more than 4 K and the intensity of the SAH greatly weakened.

The TP's unique low-level convergence/upper-level divergence structure is considered to lift water vapor and affect the YRD by the eastward movement of the prevailing westerly winds in the middle and upper levels.

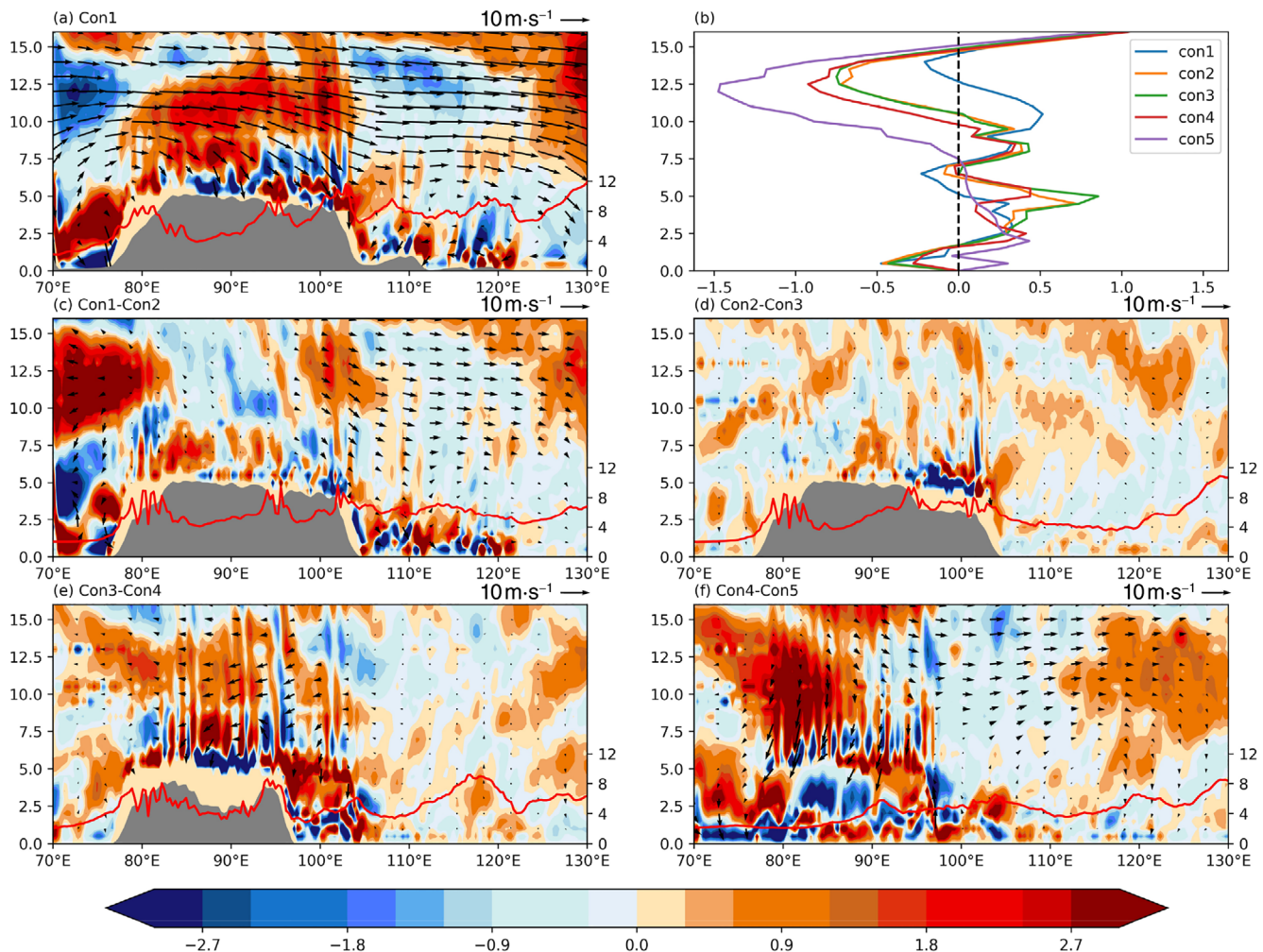


FIGURE 10 Different between the average divergences (10^{-4} s^{-1}) of the longitudinal vertical distribution (km). Vertical variation distribution of the longitudinal divergence (b); the red line in the figure shows the daily mean precipitation (mm day^{-1}) of the longitudinal distribution. The grey area is the longitudinal distribution of topography (km) (the average latitude is $28^\circ\text{--}32^\circ\text{N}$)

Therefore, we calculated the TP's longitudinal divergence and vertical velocity distribution toward the YRD (Figure 10). Moreover, precipitation is produced by the combined effect of horizontal airflow and vertical velocity. Horizontal airflow determines the humidity of the atmospheric column, while vertical velocity leads to the formation of clouds. In general, the strongest upward motion accompanies areas of concentrated precipitation. Therefore, vertical velocity is also a critical controlling factor for rainfall.

The average divergence and vertical circulation fields in the $28^\circ\text{--}32^\circ\text{N}$ longitude direction are shown in Figure 10. The convergence layer between 70°E and 80°E in Con1 extends up to 5 km (Figure 10a). Between 10 and 14 km, there is a divergent layer followed by a weak convergent layer. The lower convergent layer does not provide sufficient air replenishment to the upper layer. This

leads to a weak vertical upward motion of the air column and a shallow development of the convective system. Ding *et al.* (2021a) found that wind speed below 3,600 m is weakly dependent on elevation. However, above 3,600 m, the wind speed increases significantly with elevation. The strongest uplift occurs at 4–5 km in front of the large terrain, while the middle and lower layers exhibit subsidence motion. The sinking motion of the middle and lower layers impedes the development of convection and promotes the generation of precipitation, which forms in large quantities at the leading edge of the sizable terrain area. The dynamical and thermal effects of water vapor introduced from the TP together form a mutual feedback and promote the formation of convective clouds.

At the same time, precipitation is formed during ascent. In the central part of the TP, the ETP has a strong

convergence zone, which favours the further rise of water vapor and produces precipitation in the ETP. Chen *et al.* (2021) explained that in the thin atmospheric column over the large topography of the ETP, most of the clouds are confined to approximately 10 km. The ETP has the largest amount of convective clouds in summer, which is associated with large scale water vapor transport and strong surface heating of the TP. It also facilitates the eastward migration of convective clouds and the maintenance and development of low-pressure systems in the TP. This is consistent with the findings in the previous sections. The removal of topographic barriers enhances the upper-level dispersion in the western part of the TP (Figure 10b) and enhances the TP transport downstream (Figure 10c). In contrast, the TPSA has less influence on the meridional profile and circulation (Figure 10d). When only the role of the TP platform is considered (Figure 10e), similar to the previous analysis at different levels in the troposphere, the TP platform produces a significant heating effect over the TP, causing water vapor lifting and convergence. However, the southern slope favours the development of a subtropical ridge, which facilitates water vapor transport to the YRD (Figure 10f). Combined with the previous analysis, the vertical distribution of dispersion is considered (Figure 10b). With the removal of the topography, the dispersion of the upper subtropical layer is enhanced, accompanied by the development and enhancement of the mid-latitude ridges. There results suggest that topographic uplift is beneficial to the eastward development of convection in the ETP to the YRD. Combined with the results in section 3.3, the elimination of topography reduces the convective clouds in the ETP, and the convection and precipitation in the YRD are dominated by the contribution from the southeast coast.

3.5 | Correlation verification

During summer, the water vapor transport structure in eastern China is influenced not only by the southeast water vapor transport from the western edge of the western Pacific subtropical high-pressure system and the southwest monsoon water vapor transport from the middle and low latitudes, but also by the fluctuation of the mid-high-latitude westerly belt ridge. Upstream water vapor transport from the low-latitude ocean is an important component of precipitation in the YRD (Yanai and Wu, 2006; Wu *et al.*, 2012a). Xu *et al.* (2002) suggested that the large topographic effect of water vapor transport from the upstream low-latitude ocean is a key link in exploring the causes of plum rain and its continuous precipitation in the YRD. According to the analysis in the previous sections, the water vapor transported by the

low-latitude ocean and the TP has different effects on precipitation in CEC and SEC.

The correlation analysis with 99% confidence test between the precipitation at the CEC and SEC grid points in Con1 with and the average IVT in East Asia is shown in (Figure 11). The high IVT area is mainly concentrated in the low-latitude ocean. On the one hand, the SAH forms a significant water vapour convergence and enhances the northern branch of the SASM, resulting in upward transport of water vapor from the south slope to the TP and YRD. On the other hand, the southern branch of SASM and the southwesterly flow from the Bay of Bengal converge in the South China Sea, bringing more precipitation to the YRD. There is a significant correlation between the daily mean precipitation and the IVT of CEC and SEC. There is a significant positive correlation between the precipitation of CEC and the SASM, and a slight correlation with the southeast ocean. Thus, there is also a particular influence on precipitation and southeast ocean transport in CEC. However, the correlation between SEC and the TP is low and only positive with the correlation between the southern Himalayas along the southern part of the Himalayas and the high pressure in the South China Sea. Depending on the direction and magnitude of the IVT, SEC is dominated by water vapor from the southeast ocean, with relatively little water vapour from the TP.

Figure 12 shows the spatial distribution of the correlation between the daily mean precipitation and IVT for CEC and SEC of Con2-5, as well as the difference field of the IVT. When the slight topographic uplift is removed, the SASM northern branch carries less variation in water vapor into the TP (Figure 12a). However, the SASM carries more water vapor along the Yunnan region of China to the YRD, resulting in a higher increase in the IVT in the downstream region of the TP. For SEC, precipitation in SEC area is mainly positively correlated with SASM transport area. For CEC, a positive correlation can be clearly seen in the band originating from the TP to CEC near 30°N, with some contribution from mid-latitude IVT transport (Figure 12b). Although the IVT increases in both regions, it has less of an increase in precipitation impact (Figure 5a) and only increases convective cloudiness in the CEC (Figure 7a). After removing the TPSA, more IVT enters the TP downstream along the Yunnan (Figure 12c). Compared with Con2, the IVT increases more in the SEC (Figure 12c). The band of the positive correlation zone in CEC moves northward (Figure 12d). Dong (2018) performed a previous analysis and found that the TPSA affects downstream CEC transport. Combined with the previous analysis, it shows that TPSA has some influence on the water vapour transport path, which favours the increase in precipitation and

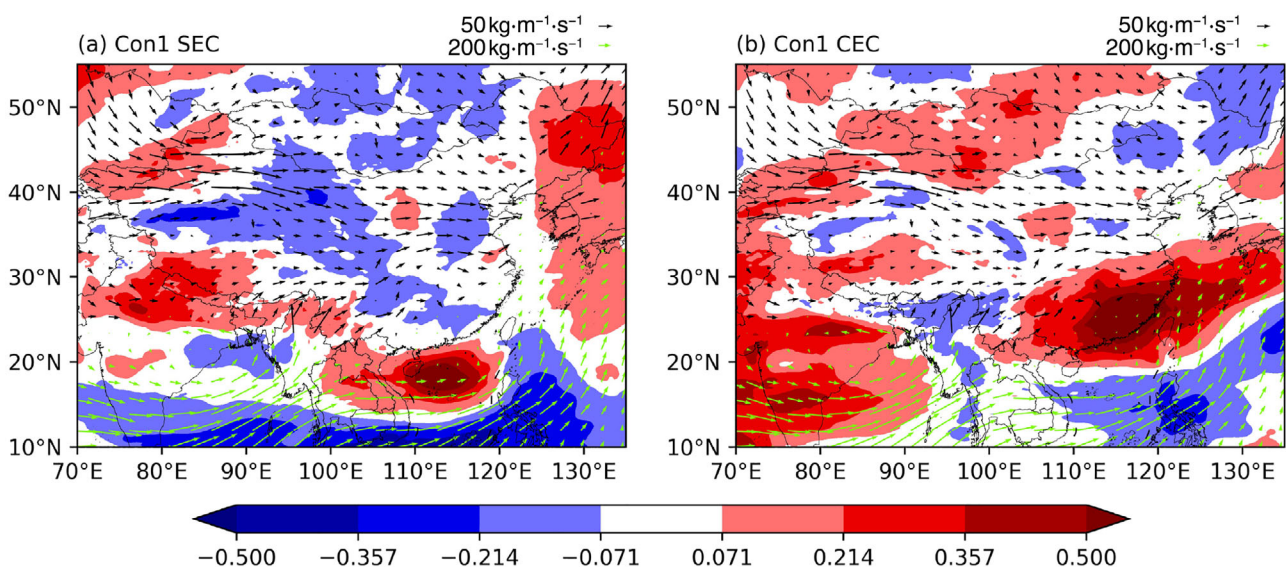


FIGURE 11 (a, b) Correlation coefficient field of control experiment Con1 between the IVT and hourly precipitation in CEC and SEC. The shaded area denotes the 99% confidence interval from the significance test and the IVT ($\text{kg}\cdot\text{m}^{-1}\cdot\text{s}^{-1}$). The IVT above $200 \text{ kg}\cdot\text{m}^{-1}\cdot\text{s}^{-1}$ is expressed by green arrows, and labelled as $50 \text{ kg}\cdot\text{m}^{-1}\cdot\text{s}^{-1}$

convective clouds in the SEC region. The removal of the TP platform favours the transport of the IVT in the mid-latitudes (Figure 12e), but the southern slope of TP has a resistive effect on the transport of the northern branch of the SASM. The mid-latitudes excite the anomalous convergence and dispersion of water vapor, consistent with the troposphere of the generated cyclone and anticyclone anomalies (Figures 5c and 7c). This is consistent with the previous analysis that the presence of the southern slope of the TP facilitates transport downstream, while the main role of the TP platform is manifested in the local heating to produce lifting. After removing all topography, water vapor has a contribution from the low-latitude thermal low-pressure area in the South China Sea to the southeast to northwest China in addition to the SASM transport, and the contribution of the TP to downstream transport is reduced (Figure 12g). The SEC exhibits higher oceanic water vapor transport and shows a significant negative correlation with mid-latitude transport (Figure 12h). The CEC exhibits a positive correlation with low-latitude transport in addition to the mid-latitude water vapor dissipation centres.

The absence of the TP leads to the interaction of dry air at mid-latitudes with wet airflow transported at low latitudes. The removal of topography favours the convergence and dispersion of mid-latitude water vapor, while the water vapor transported downstream from Yunnan contributes to the anomalous convergence of water vapor in northeastern China. The mid-latitude dynamical anomaly may have formed a confrontation with the low-latitude dynamical system. Due to the forced removal of

the topography, although the water vapor entering the downstream increases, it leads to the inefficient process of precipitation and the convective generation process, which may be the reason for the southward shift of the precipitation zone to approximately 20°N.

Taken together, the climate systems that directly or indirectly affect the TP appear to work together in a dynamic manner, and precipitation, convective cloudiness, and water vapor transport in the TP and its downstream regions cannot be attributed entirely to one climate system. Ding *et al.* (2021b) found that a weakening-related southerly shift of the westerly ripples occurs due to weakening summer winds. Weakened westerly winds result in attenuated water vapor transport to the southeast from the south and west. It also reports that YRD precipitation anomalies contribute not only to the movement of the SAH but also to global telecorrelation in East Asia (e.g., Wei *et al.*, 2015).

4 | CONCLUSIONS AND DISCUSSION

Initially, Manabe and Terpstra (1974) and Kutzbach *et al.* (1989) conducted natural terrain and mountain-free experiments through low-resolution climate models to roughly explore the influence of TP topography on climate. Subsequently, high-resolution block studies on the effect of TP topography uplift on climate were conducted (Tang *et al.*, 2012; Zhang *et al.*, 2015; Yu *et al.*, 2018). Based on previous studies, the summer of 2011–2020 was

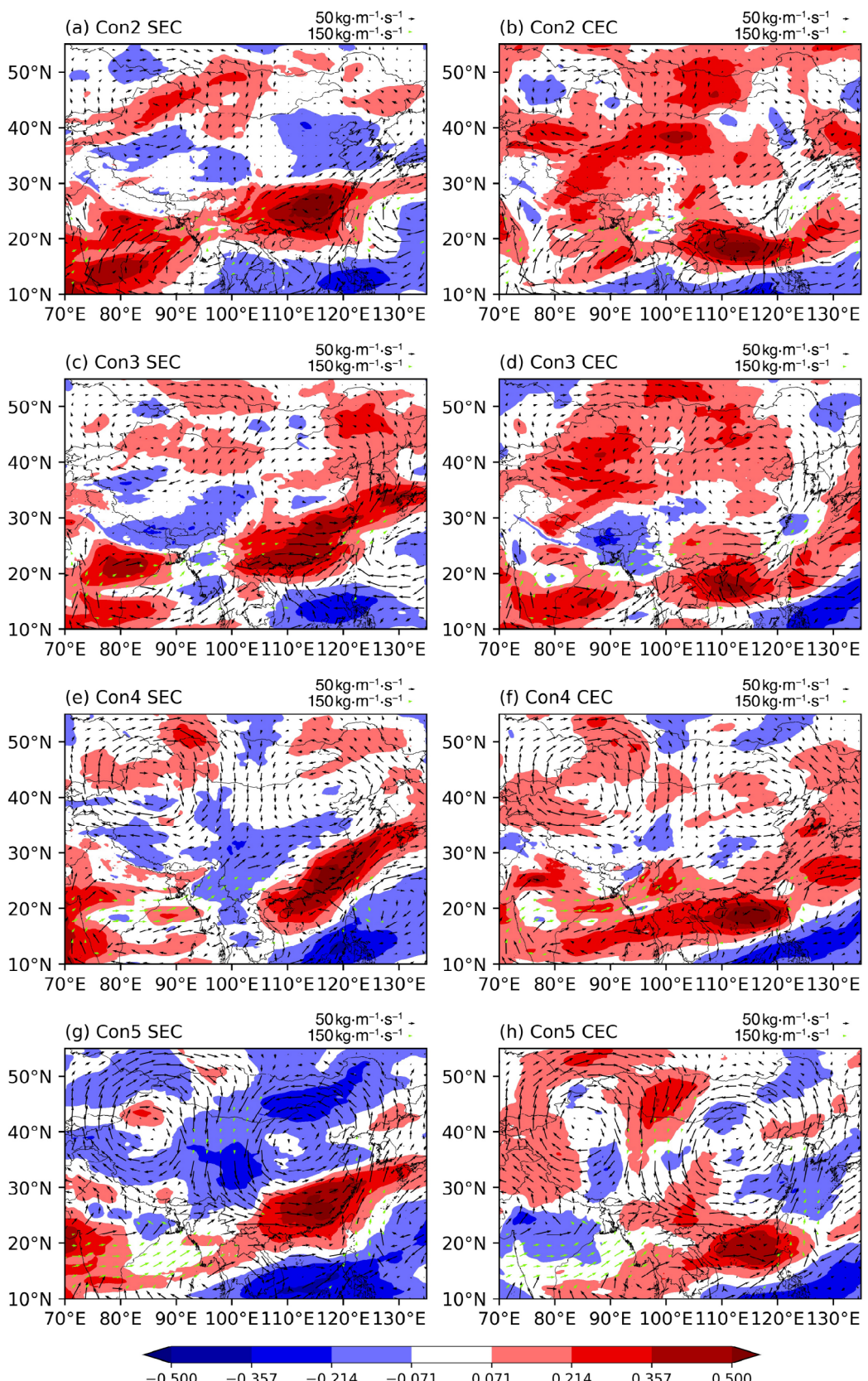


FIGURE 12 Correlation coefficient field between the IVT of Con2, Con3, Con4, Con5, and hourly precipitation in SEC and CEC in the sensitivity experiment. The shaded area is the 99% confidence interval of the IVT through the significance test. Difference the IVT circulation between the sensitivity experiment and Con1 ($\text{kg}\cdot\text{m}^{-1}\cdot\text{s}^{-1}$). The IVT above $150 \text{ kg}\cdot\text{m}^{-1}\cdot\text{s}^{-1}$ is expressed by green arrows, and labelled as $50 \text{ kg}\cdot\text{m}^{-1}\cdot\text{s}^{-1}$

selected as the study for sensitivity experiments on the regional uplift of the TP using the WRF model. The climate response to different regional uplifts of the TP was investigated for the summer climate of the ETP, SEC and CEC.

The topographic uplift of the TP has an excitation effect in East Asia during summer. TP topography has an excitation effect on the generation and development of low-level cyclonic high disturbances in the SAH. At the same time, it has a suppressive effect on the generation and development of cyclones and anticyclones in the mid-latitudes. The presence of the TP is favourable to the uplift of low-level water vapour in the local area, while the presence of the southern slope is favourable to the maintenance and development of the SAH and mid-latitude anomalous circulation. The precipitation belt moves southward, and there is a tendency for precipitation to decrease over most of China. The presence of the TP enhances the SAH such that the precipitation in northern India and the Bay of Bengal shows positive anomalies. Condensation heating in the precipitation centre produces SAH low-level cyclonic circulation in the lower layer and further enhances the SASM, which implies positive feedback between precipitation and circulation.

The presence of large TP topography, under the influence of topography and the unique water tower effect of the TP, lifts the warm and humid airflow to form clouds, which facilitates the formation of convective cloud masses and their transport to the YRD. The uplifting effect of the TP platform has an impact on the formation of convective clouds, while the southern slope of the TP is manifested in maintaining the SAH. Meanwhile, the disturbance of the southern slope can cause the generation of low-pressure troughs and the generation and development of high-pressure ridges in the lower mid-latitude or downstream, which is conducive to the downstream transmission of convective clouds in the radial direction and has an impact on the weather situation in East Asia.

The large topography of the TP favours the heating effect in the upper troposphere. Removing the topographic perturbation is conducive to increasing the anomalous cyclonic heating effect in northeast China, suppressing the heating effect in the main body of the TP and greatly weakening the SAH intensity. At the same time, it influences the generation and development of the upper tropospheric trough ridge and favours the generation and development of upper mid-latitude anomalous cyclone anticyclones. The platform heating of the TP plays an important role in the warming of the upper layers and maintains the location of the warm centre over the TP. The heating effect of the TP in the upper

level shows a wider range in the upper level, covering the whole TP area, and is more intense than the heating of the southern slope of the TP. The southern slope of the TP makes an important contribution to the circulation in the upper layers. An anomalous anticyclonic cold centre is excited for the northeastern part of China, while the southern slope also has a certain warming effect on the upper layers of the SAH. The removal of topographic barriers strengthens the upper level dispersion in the western part of the TP and enhances TP transport downstream. The TPSA, on the other hand, has less of an influence on the meridional profile and circulation. Topographic uplift favours the eastward development of convection from the ETP to the YRD.

Water vapor originating from the eastward movement of the TP is mainly transported to CEC and generates precipitation, while the supply of water vapor in the SEC is mainly derived from transport along the southeast coast. After removing the topographic disturbance, the SASM carries more water vapor along the Yunnan of China to the YRD, resulting in a higher increase in the IVT in the downstream area of the TP. The SEC exhibits a higher oceanic water vapor transport and shows a significant negative correlation with mid-latitude transport. The CEC shows a positive correlation with low-latitude transport in addition to the mid-latitude water vapor dispersion centre. The TPSA has an influence on water vapor transport. There is some influence on the path, which favours an increase in precipitation and convective clouds in the SEC. The removal of topography favours the convergence and dispersion of mid-latitude water vapor, while the water vapor transported from Yunnan downstream contributes to the anomalous convergence of water vapor in northeast China. The mid-latitude dynamical anomaly may form a confrontation with the low-latitude dynamical system. Due to the forced removal of topography, although the water vapor entering downstream increases, it leads to inefficient precipitation and convective generation processes, which may be the reason for the southward shift of the precipitation belt to approximately 20°N.

Despite the advantages of our simulations compared with previous studies, there are still some limitations and uncertainties:

First, there are limitations in the terrain modification process in this research. The experiments resulted in large decline rates at the edges of the slopes. Despite terrain smoothing, the operation may lead to instability and uncertainty in the climate model. Second, in addition to dynamic and thermal effects, substances such as aerosols also have a potential role in the formation and development of clouds and precipitation (Zhao *et al.*, 2021). Nevertheless, the simulation of East Asia using the WRF

model can be still used to discuss the influence of TP topography on the Asian monsoon system and explore the topographic response to climate.

ACKNOWLEDGEMENTS

This study was supported under the National Science Foundation of China (Grant Nos. 42075067, 42075068 and 41875071), the Second Tibetan Plateau Scientific Expedition and Research (STEP) program (Grant No. 2019QZKK0105), the Natural Science Foundation of Jiangsu Province (Grant No. BK20170945), Abu Dhabi, UAE under the UAE Research Program for Rain Enhancement Science.

ORCID

Kai Yang  <https://orcid.org/0000-0003-3295-7926>

REFERENCES

- Abe, M., Kitoh, A. and Yasunari, T. (2003) An evolution of the Asian summer monsoon associated with mountain uplift-simulation with the MRI atmosphere-ocean coupled GCM. *Journal of the Meteorological Society of Japan. Series II*, 81(5), 909–933. <https://doi.org/10.2151/jmsj.81.909>.
- Ashfaq, M. (2020) Topographic controls on the distribution of summer monsoon precipitation over South Asia. *Earth Systems and Environment*, 4(4), 667–683. <https://doi.org/10.1007/s41748-020-00196-0>.
- Bai, J. and Xu, X. (2004) Atmospheric hydrological budget with its effects over Tibetan Plateau. *Journal of Geographical Sciences*, 14(S1), 81–86. <https://doi.org/10.1007/BF02873094>.
- Boos, W. and Kuang, Z. (2010) Dominant control of the South Asian monsoon by orographic insulation versus plateau heating. *Nature*, 463(7278), 218–222. <https://doi.org/10.1038/nature08707>.
- Cavazos, T., Luna-Niño, R., Cerezo-Mota, R., Fuentes-Franco, R., Méndez, M., Pineda Martínez, L. and Valenzuela, E. (2019) Climatic trends and regional climate models intercomparison over the CORDEX-CAM (Central America, Caribbean, and Mexico) domain. *International Journal of Climatology*, 40(3), 1396–1420. <https://doi.org/10.1002/joc.6276>.
- Chen, B., Zhang, W., Yang, S. and Xu, X. (2019) Identifying and contrasting the sources of the water vapor reaching the subregions of the Tibetan Plateau during the wet season. *Climate Dynamics*, 53, 6891–6907. <https://doi.org/10.1007/s00382-019-04963-2>.
- Chen, J. and Bordoni, S. (2014) Orographic effects of the Tibetan Plateau on the East Asian summer monsoon: an energetic perspective. *Journal of Climate*, 27(8), 3052–3072.
- Chiodi, A. and Harrison, D. (2010) Characterizing warm-ENSO variability in the equatorial Pacific: an OLR perspective. *Journal of Climate*, 23(9), 2428–2439. <https://doi.org/10.1175/2009jcli3030.1>.
- Cordeira, J., Ralph, F. and Moore, B. (2013) The development and evolution of two atmospheric rivers in proximity to western North Pacific tropical cyclones in October 2010. *Monthly Weather Review*, 141(12), 4234–4255. <https://doi.org/10.1175/mwr-d-13-00019.1>.
- Ding, J., Cuo, L., Zhang, Y. and Zhang, C. (2021a) Varied spatiotemporal changes in wind speed over the Tibetan Plateau and its surroundings in the past decades. *International Journal of Climatology*, 41(13), 5956–5976. <https://doi.org/10.1002/joc.7162>.
- Ding, J., Cuo, L., Zhang, Y., Zhang, C., Liang, L. and Liu, Z. (2021b) Annual and seasonal precipitation and their extremes over the Tibetan Plateau and its surroundings in 1963–2015. *Atmosphere*, 12(5), 620. <https://doi.org/10.3390/atmos12050620>.
- Ding, Y. (1993) *Research on the Persistent Heavy Rainfall in the Yangtze River and Huaihe River Valleys in 1991*. Beijing: China Meteorological Press.
- Ding, Y. and Johnny, C. (2005) The East Asian summer monsoon: an overview. *Meteorology and Atmospheric Physics*, 89(1), 117–142. <https://doi.org/10.1007/s00703-005-0125-z>.
- Dong, L. (2018) *The impact of land-atmosphere processes over the “sensitivity area” of the Tibetan Plateau and moisture transport on Meiyu precipitation over the middle and lower Yangtze River*. PhD dissertation.
- Duan, A. and Wu, G. (2005) Role of the Tibetan Plateau thermal forcing in the summer climate patterns over subtropical Asia. *Climate Dynamics*, 24(7–8), 793–807. <https://doi.org/10.1007/s00382-004-0488-8>.
- Duan, A., Sun, R. and He, J. (2017) Impact of surface sensible heating over the Tibetan Plateau on the western Pacific subtropical high: a land–air–sea interaction perspective. *Advances in Atmospheric Sciences*, 34(2), 157–168. <https://doi.org/10.1007/s00376-016-6008-z>.
- He, B. (2012) Numerical simulation and mechanism study on the impacts of Tibetan Plateau thermodynamic forcing over South Asian summer monsoon.
- Hersbach, H., Bell, B., Berrisford, P., Hirahara, S., Horányi, A., Muñoz-Sabater, J., Nicolas, J., Peubey, C., Radu, R., Schepers, D., Simmons, A., Soci, C., Abdalla, S., Abellan, X., Balsamo, G., Bechtold, P., Biavati, G., Bidlot, J., Bonavita, M., Chiara, G., Dahlgren, P., Dee, D., Diamantakis, M., Dragani, R., Flemming, J., Forbes, R., Fuentes, M., Geer, A., Haimberger, L., Healy, S., Hogan, R.J., Hólm, E., Janisková, M., Keeley, S., Laloyaux, P., Lopez, P., Lupu, C., Radnoti, G., Rosnay, P., Rozum, I., Vamborg, F., Villaume, S. and Thépaut, J.N. (2020) The ERA5 global reanalysis. *Quarterly Journal of the Royal Meteorological Society*, 146(730), 1999–2049. <https://doi.org/10.1002/qj.3803>.
- Hong, S.Y. and Lim, J. (2006) The WRF single-moment 6-class microphysics scheme (WSM6). *Asia-Pacific Journal of Atmospheric Sciences*, 42(2), 129–151.
- Hong, S., Noh, Y. and Dudhia, J. (2006) A new vertical diffusion package with an explicit treatment of entrainment processes. *Monthly Weather Review*, 134(9), 2318–2341. <https://doi.org/10.1175/mwr3199.1>.
- Iacono, M., Delamere, J., Mlawer, E., Shephard, M., Clough, S. and Collins, W. (2008) Radiative forcing by long-lived greenhouse gases: calculations with the AER radiative transfer models. *Journal of Geophysical Research*, 113(D13), D13103. <https://doi.org/10.1029/2008jd009944>.
- James, C. and Houze, R. (2005) Modification of precipitation by coastal orography in storms crossing northern California.

- Monthly Weather Review*, 133(11), 3110–3131. <https://doi.org/10.1175/mwr3019.1>.
- Kain, J. (2004) The Kain–Fritsch convective parameterization: an update. *Journal of Applied Meteorology*, 43(1), 170–181. [https://doi.org/10.1175/1520-0450\(2004\)043<0170:TKCPAU>2.0.CO;2](https://doi.org/10.1175/1520-0450(2004)043<0170:TKCPAU>2.0.CO;2).
- Kang, Y. and Gong, Y. (2021) Diurnal variation characteristics of summer convection over the Qinghai-Xizang Plateau and South Asia area based on the high-resolution OLR data. *Plateau Meteorology*, 40(3), 472–485. <https://doi.org/10.7522/j.issn.1000-0534.2020.00105>.
- Krishnamurti, T., Daggupaty, S., Fein, J., Kanamitsu, M. and Lee, J. (1973) Tibetan high and upper tropospheric tropical circulations during northern summer. *Bulletin of the American Meteorological Society*, 54(12), 1234–1250. <https://doi.org/10.1175/1520-0477-54.12.1234>.
- Kutzbach, J., Guetter, P., Ruddiman, W. and Prell, W. (1989) Sensitivity of climate to late Cenozoic uplift in southern Asia and the American west: numerical experiments. *Journal of Geophysical Research*, 94(D15), 18393. <https://doi.org/10.1029/jd094id15p18393>.
- Li, D., Yang, K., Tang, W., Li, X., Zhou, X. and Guo, D. (2020) Characterizing precipitation in high altitudes of the western Tibetan Plateau with a focus on major glacier areas. *International Journal of Climatology*, 40, 5114–5127. <https://doi.org/10.1002/joc.6509>.
- Liu, X. and Yin, Z. (2002) Sensitivity of East Asian monsoon climate to the uplift of the Tibetan Plateau. *Palaeogeography, Palaeoclimatology, Palaeoecology*, 183(3–4), 223–245. [https://doi.org/10.1016/s0031-0182\(01\)00488-6](https://doi.org/10.1016/s0031-0182(01)00488-6).
- Liu, Y., Bao, Q., Duan, A., Qian, Z. and Wu, G. (2007) Recent progress in the impact of the Tibetan Plateau on climate in China. *Advances in Atmospheric Sciences*, 24(6), 1060–1076. <https://doi.org/10.1007/s00376-007-1060-3>.
- Liu, Y., Wang, Z., Zhuo, H. and Wu, G. (2017) Two types of summertime heating over Asian large-scale orography and excitation of potential vorticity forcing II. Sensible heating over Tibetan Iranian Plateau. *Science China Earth Sciences*, 60, 733–744. <https://doi.org/10.1007/s11430-016-9016-3>.
- Liu, Y., Wu, G., Hong, J., Dong, B., Duan, A., Bao, Q. and Zhou, L. (2012) Revisiting Asian monsoon formation and change associated with Tibetan Plateau forcing: II. Change. *Climate Dynamics*, 39(5), 1183–1195. <https://doi.org/10.1007/s00382-012-1335-y>.
- Lu, C., Yu, G. and Xie, G. (2005) Tibetan Plateau serves as a water tower. In: *IEEE International Geoscience & Remote Sensing Symposium*. IEEE. <https://doi.org/10.1109/IGARSS.2005.1526498>
- Luo, H. and Yanai, M. (1983) The large-scale circulation and heat sources over the Tibetan Plateau and surrounding areas during the early summer of 1979. Part I: precipitation and kinematic analyses. *Monthly Weather Review*, 111(5), 922–944. [https://doi.org/10.1175/1520-0493\(1983\)111<0922:tlscdh>2.0.co;2](https://doi.org/10.1175/1520-0493(1983)111<0922:tlscdh>2.0.co;2).
- Manabe, S. and Terpstra, T. (1974) The effects of mountains on the general circulation of the atmosphere as identified by numerical experiments. *Journal of the Atmospheric Sciences*, 31(1), 3–42. [https://doi.org/10.1175/1520-0469\(1974\)031<0003:teomot>2.0.co;2](https://doi.org/10.1175/1520-0469(1974)031<0003:teomot>2.0.co;2).
- Martin, F., Paul, J., Neiman, G. and Wick, A. (2004) Satellite and CALJET aircraft observations of atmospheric Rivers over the eastern North Pacific Ocean during the winter of 1997/98. *Monthly Weather Review*, 132(7), 1721–1745. [https://doi.org/10.1175/1520-0493\(2004\)132<1721:sacaho>2.0.co;2](https://doi.org/10.1175/1520-0493(2004)132<1721:sacaho>2.0.co;2).
- Mason, R. and Anderson, C. (1963) The development and decay of the 100-MB. Summertime anticyclone over southern Asia. *Monthly Weather Review*, 91(1), 3–12. [https://doi.org/10.1175/1520-0493\(1963\)091<0003:TDADOT>2.3.CO;2](https://doi.org/10.1175/1520-0493(1963)091<0003:TDADOT>2.3.CO;2).
- Miao, Q., Xu, X. and Shi, X. (2004) Water vapor transport structure of anomalous rainy centers in the ambient area of Tibetan Plateau. *Meteorological Monthly*, 30(12), 44–47. <https://doi.org/10.7519/j.issn.1000-0526.2004.12.010>.
- Molnar, P., Boos, W. and Battisti, D. (2010) Orographic controls on climate and paleoclimate of Asia: thermal and mechanical roles for the Tibetan Plateau. *Annual Review of Earth and Planetary Sciences*, 38(1), 77–102. <https://doi.org/10.1146/annurev-earth-040809-152456>.
- Neiman, P., Ralph, F., Wick, G., Lundquist, J. and Dettinger, M. (2008) Meteorological characteristics and overland precipitation impacts of atmospheric rivers affecting the west coast of North America based on eight years of SSM/I satellite observations. *Journal of Hydrometeorology*, 9(1), 22–47. <https://doi.org/10.1175/2007JHM855.1>.
- Pan, Y., Shen, Y. and Yu, J. (2012) Analysis of the combined gauge-satellite hourly precipitation over China based on the OI technique. *Acta Meteorologica Sinica*, 70(6), 1381–1389. <https://doi.org/10.11676/qxb2012.116>.
- Park, T., Ho, C., Jeong, J., Heo, J. and Deng, Y. (2015) A new dynamical index for classification of cold surge types over East Asia. *Climate Dynamics*, 45(9–10), 2469–2484. <https://doi.org/10.1007/s00382-015-2483-7>.
- Shen, Y., Zhao, P., Pan, Y. and Yu, J. (2014) A high spatiotemporal gauge-satellite merged precipitation analysis over China. *Journal of Geophysical Research: Atmospheres*, 119(6), 3063–3075. <https://doi.org/10.1002/2013JD020686>.
- Skamarock, W.C., Klemp, J.B., Dudhia, J., Gill, D.O., Liu, Z., Berner, J., Wang, W., Powers, J.O., Duda, M.G., Barker, D.M. and Hang, X. (2019) *A description of the advanced research WRF model version 4*. Boulder, CO: NCAR/UCAR. <https://doi.org/10.5065/1dfh-6p97>.
- Skamarock, W.C., Klemp, J.B., Dudhia, J., Gill, D.O., Barker, D., Duda, M.G., Hang, X., Wang, W. and Powers, J.O. (2008) *A description of the advanced research WRF version 3* (No. NCAR/TN-475+STR). Boulder, CO: University Corporation for Atmospheric Research. <https://doi.org/10.5065/D68S4MVH>.
- Sun, J. and Zhang, F. (2012) Impacts of Mountain–Plains solenoid on diurnal variations of rainfalls along the Mei-Yu front over the East China Plains. *Monthly Weather Review*, 140(2), 379–397. <https://doi.org/10.1175/MWR-D-11-00041.1>.
- Tang, H., Micheels, A., Eronen, J., Ahrens, B. and Fortelius, M. (2012) Asynchronous responses of East Asian and Indian summer monsoons to mountain uplift shown by regional climate modelling experiments. *Climate Dynamics*, 40(5–6), 1531–1549. <https://doi.org/10.1007/s00382-012-1603-x>.
- Tewari, M., Chen, F., Wang, W., Dudhia, J., Lemone, M.A., Mitchell, K., Ek, M., Gayno, G., Wegiel, J. and Cuenca, R.H. (2004) *Implementation and verification of the united NOAH land surface model in the WRF model*. Paper presented at 20th Conference on Weather Analysis and Forecasting/16th Conference on Numerical Weather Prediction. Available at: http://ams.confex.com/ams/84Annual/techprogram/paper_69061.htm.

- Wang, B., Bao, Q., Hoskins, B., Wu, G. and Liu, Y. (2008) Tibetan Plateau warming and precipitation changes in East Asia. *Geophysical Research Letters*, 35(14), L14702.
- Wang, C., Shi, H., Hu, H., Wang, Y. and Xi, B. (2015) Properties of cloud and precipitation over the Tibetan Plateau. *Advances in Atmospheric Sciences*, 32(11), 1504–1516. <https://doi.org/10.1007/s00376-015-4254-0>.
- Wang, X., Tolksdorf, V., Otto, M. and Scherer, D. (2020) WRF-based dynamical downscaling of ERA5 reanalysis data for High Mountain Asia: towards a new version of the High Asia refined analysis. *International Journal of Climatology*, 41(1), 743–762. <https://doi.org/10.1002/joc.6686>.
- Wang, Z. and Zeng, X. (2008) Snow Albedo's dependence on solar zenith angle from in situ and MODIS data. *Atmospheric and Oceanic Science Letters*, 1(1), 45–50. <https://doi.org/10.1080/16742834.2008.11446763>.
- Wang, Z., Duan, A. and Wu, G. (2013) Time-lagged impact of spring sensible heat over the Tibetan Plateau on the summer rainfall anomaly in east China: case studies using the WRF model. *Climate Dynamics*, 42(11–12), 2885–2898. <https://doi.org/10.1007/s00382-013-1800-2>.
- Wei, W., Zhang, R., Wen, M., Kim, B. and Nam, J. (2015) Interannual variation of the South Asian high and its relation with Indian and East Asian summer monsoon rainfall. *Journal of Climate*, 28(7), 2623–2634. <https://doi.org/10.1175/jcli-d-14-00454.1>.
- Wu, G., Duan, A., Liu, Y., Mao, J., Ren, R., Bao, Q., He, B., Liu, B. and Hu, W. (2014) Tibetan Plateau climate dynamics: recent research progress and outlook. *National Science Review*, 2(1), 100–116. <https://doi.org/10.1093/nsr/nwu045>.
- Wu, G., Liu, Y., Dong, B., Liang, X., Duan, A., Bao, Q. and Yu, J. (2012a) Revisiting Asian monsoon formation and change associated with Tibetan Plateau forcing: I. Formation. *Climate Dynamics*, 39(5), 1169–1181. <https://doi.org/10.1007/s00382-012-1334-z>.
- Wu, G., Liu, Y., He, B., Bao, Q., Duan, A. and Jin, F. (2012b) Thermal controls on the Asian summer monsoon. *Scientific Reports*, 2(1), 404. <https://doi.org/10.1038/srep00404>.
- Wu, G., Liu, Y., Zhang, Q., Duan, A., Wang, T., Wan, R., Liu, X., Li, W., Wang, Z. and Liang, X. (2007) The influence of mechanical and thermal forcing by the Tibetan Plateau on Asian climate. *Journal of Hydrometeorology*, 8(4), 770–789. <https://doi.org/10.1175/JHM609.1>.
- Wu, G., Zhuo, H., Wang, Z. and Liu, Y. (2016a) Two types of summertime heating over the Asian large-scale orography and excitation of potential-vorticity forcing I. Over Tibetan Plateau. *Science China Earth Sciences*, 59(10), 1996–2008. <https://doi.org/10.1007/s11430-016-5328-2>.
- Wu, S., Liu, Y., Zou, X. and Wu, G. (2016b) The simulation analysis of the precipitation over the southern slopes of the Tibetan Plateau based on the WRF model. *Acta Meteorologica Sinica*, 74(5), 744–756. <https://doi.org/10.11676/qxb2016.048>.
- Xu, J., Wang, H. and Li, H. (2014) Preliminary simulation analysis of moisture budget over Qinghai-Xizang plateau in summer. *Plateau Meteorology*, 33(5), 1173–1181. <https://doi.org/10.7522/j.issn.1000-0534.2013.00117>.
- Xu, X., Dong, L. and Zhao, Y. (2019) Effect of the Asian water tower over the Qinghai-Tibet Plateau and the characteristics of atmospheric water circulation. *Chinese Science Bulletin*, 64(27), 2830–2841. <https://doi.org/10.1360/TB-2019-0203>.
- Xu, X., Lu, C., Ding, Y., Shi, X., Guo, Y. and Zhu, W. (2013) What is the relationship between China summer precipitation and the change of apparent heat source over the Tibetan Plateau? *Atmospheric Science Letters*, 14, 227–234. <https://doi.org/10.1002/asl2.444>.
- Xu, X., Lu, C., Shi, X. and Gao, S. (2008) World water tower: an atmospheric perspective. *Geophysical Research Letters*, 35(20), L20815. <https://doi.org/10.1029/2008GL035867>.
- Xu, X., Tao, S. and Wang, J. (2002) The relationship between water vapor transport features of Tibetan Plateau-monsoon “large triangle” affecting region and drought-flood abnormality of China. *Acta Meteorologica Sinica*, 60(3), 257–266. <https://doi.org/10.11676/qxb2002.032>.
- Xu, X., Zhao, T., Shi, X. and Lu, C. (2015) A study of the role of the Tibetan Plateau's thermal forcing in modulating rainband and moisture transport in eastern China. *Acta Meteorologica Sinica*, 73(1), 20–35. <https://doi.org/10.11676/qxb2014.051>.
- Yanai, M. and Wu, G. (2006) Effects of the Tibetan Plateau. In: *The Asian Monsoon*. Berlin, HD: Springer Praxis Books, pp. 513–549. https://doi.org/10.1007/3-540-37722-0_13.
- Yanai, M., Li, C. and Song, Z. (1992) Seasonal heating of the Tibetan Plateau and its effects on the evolution of the Asian summer monsoon. *Journal of the Meteorological Society of Japan. Series II*, 70(1B), 319–351. https://doi.org/10.2151/jmsj1965.70.1B_319.
- Yeh, T. (1950) The circulation of the high troposphere over China in the winter of 1945–46. *Tellus*, 2(3), 173–183. <https://doi.org/10.1111/j.2153-3490.1950.tb00329.x>.
- Yeh, T., Gao, S., Zhou, M., et al. (1979) *Qinghai-Tibet Plateau Meteorology*. Beijing: China Science Publishing & Media Ltd.
- Yeh, T., Lo, S. and Chu, P. (1957) The wind structure and heat balance in the lower troposphere over Tibetan Plateau and its surrounding. *Acta Meteorologica Sinica*, 28(2), 108–121. <https://doi.org/10.11676/qxb1957.010>.
- Yu, E., Sun, J., Chen, H. and Xiang, W. (2014) Evaluation of a high-resolution historical simulation over China: climatology and extremes. *Climate Dynamics*, 45(7–8), 2013–2031. <https://doi.org/10.1007/s00382-014-2452-6>.
- Yu, E., Zhang, R., Jiang, D., Ramstein, G., Zhang, Z. and Sun, J. (2018) High-resolution simulation of Asian monsoon response to regional uplift of the Tibetan Plateau with regional climate model nested with global climate model. *Global and Planetary Change*, 169, 34–47. <https://doi.org/10.1016/j.gloplacha.2018.07.002>.
- Yu, J., Shen, Y. and Pan, Y. (2013) Improvement of satellite-based precipitation estimates over China based on probability density function matching method. *Journal of Applied Meteorological Science*, 24(5), 544–553. <https://doi.org/10.3969/j.issn.1001-7313.2013.05.004>.
- Zhang, M. and Jiang, Z. (2013) Analyses of high-resolution merged precipitation products over China. *Climatic and Environmental Research*, 4, 461–471. <https://doi.org/10.3878/j.issn.1006-9585.2012.12044>.
- Zhang, R., Jiang, D., Zhang, Z. and Yu, E. (2015) The impact of regional uplift of the Tibetan Plateau on the Asian monsoon climate. *Palaeogeography, Palaeoclimatology, Palaeoecology*, 417, 137–150. <https://doi.org/10.1016/j.palaeo.2014.10.030>.

- Zhao, P., Xiao, H., Liu, J. and Zhou, Y. (2021) Precipitation efficiency of cloud and its influencing factors over the Tibetan Plateau. *International Journal of Climatology*, 42(1), 416–434. <https://doi.org/10.1002/joc.7251>.
- Zhao, P., Xu, X., Chen, F., Guo, X., Zheng, X., Liu, L., Hong, Y., Li, Y., La, Z., Peng, H. and Zhong, L. (2018) The third atmospheric scientific experiment for understanding the earth-atmosphere coupled system over the Tibetan Plateau and its effects. *Bulletin of the American Meteorological Society*, 99(4), 757–776. <https://doi.org/10.1175/BAMS-D-16-0050.1>.
- Zhao, Y., 2016. Mechanism of the influence of the large-scale topography and water vapor transport structure of the Tibetan Plateau on the extreme events of heavy rainfall time and space distribution in eastern China. Chinese Academy of Meteorological Sciences. Master dissertation.
- Zhao, Y. (2018) *Evaluation and correction of TRMM 3B42 RT and CMORPH precipitation data in the region of China*. Master's thesis, Henan Polytechnic University. Master dissertation.

How to cite this article: Yang, K., Chen, J., Lu, C., Li, J., Liu, T., Deng, L., & Li, Y. (2022). Impacts of regional uplift of the Tibetan Plateau on local summer precipitation and downstream moisture budget: A simulation study. *International Journal of Climatology*, 42(16), 8882–8903. <https://doi.org/10.1002/joc.7781>